BL1A BL8B1 BL7B

Blue Shift of UV Emission Band by Inner-core Excitation on InAlGaN

S. Naoe, K. Okada*, S. Hamaura*, S. Hamada*, K. Kimura*,
K. Fukui*, H. Hirayama**

Faculty of Engineering, Kanazawa University, Ishikawa 920-1192, Japan
** Research Center for Development of Far-Infrared Region, Fukui 910-8507, Japan*
*** The Institute of Physical and Chemical Research, Wako 351-0198, Japan*

UV emission on InAlGaN where In takes a role increasing luminosity are obtained by band-to-band excitation and also by inner-core excitation. On the previous research [1], UV emission band (B band) excited by Al-K inner-core excitation showed shift of the peak position to the higher energy side with the wider half width of the band, by comparing with the B band excited by band to band energy region. This time, the measurement for N-K inner-core excitation was performed and the samples of several content of In element were examined

Experiments

A cryostat of Liq. He flow type was used, because the emission becomes remarkable at low temperature. Measurements were carried out at BL1A , BL8B1 and BL7B, for Al K core electron, N K core and band-to-band excitation regions, respectively. The luminescence was caught by an optical fiber inserted into vacuum chamber and detected by a CCD system attached to a spectrometer. This time, a hemispherical lens was set onto the tip of the optical fiber, so the intensity of signals was attained to increase by three times.

There is left an important technical problem to retain the same precision on calibrating the spectrometer among the each measurement on a different beam port, where the wavelength calibration is usually done to set a Hg lamp at the position of a sample holder, no changing the alinement of the optical system after the measurement.

The measurement to study B band in varying the luminance brightness is necessary, because the behavior of B band resembles to the case of the blue shift on semiconductors, where the blue shift is known to become on progress by increasing the luminance brightness of the excitation light. We tried measurement at such a time as just after beam injection, decrement state of beam current, preparation driving mode or single bunch driving mode of an accelerator and furthermore changed a monochromator crystal KTP to InSb or to Beta-alumina in BL1A.

Results

Results are shown in Fig.1. The B band is shown as B and the emission band in visible region as Y in the figure. The samples were grown on a substrate SiC. The exciting light becomes to reach at the substrate in proportional to the increase of the order of exciting light. The luminescence from SiC dose not existed in the energy region of B band, therefore the SiC substrate makes no matter for the study of B band. Similar results are obtained for $In_{0.05}Al_{0.12}Ga_{0.83}N$ and $In_{0.04}Al_{0.35}Ga_{0.61}N$. As seen from Fig.1, B band varies as the manner as if it would include the shape of the band itself toward to higher energy side by increasing the energy of the excitation light (4 to 400 to 1500eV). This behavior will be understood as that the band filling occurs in our samples in resemblance to the case of semiconductors.

Many electrons and holes (the order of 10^2) are produced due to the inner-core hole relaxation. They are concentrated to occupy the bottom part of conduction band or of the top part of the valence band. An electron occupied a state a little above the lowest energy state of conduction band becomes to make transition toward a hole in the valence band, emitting a photon whose energy value corresponds to the higher energy part of the B band on the axis of abscissa of luminescence spectra. Thus the blue shift of B band realizes in inner-core excitation. As the order of photon number in BL1A and BL8B1 is not enough to make band filling, then the transition will occur around the inner-core excited element before the electrons and holes fully relax to move into the whole area of the crystal.

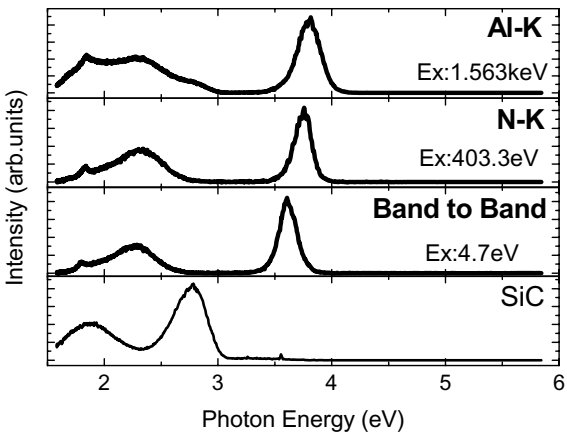

Fig. 1. UV and visible emission spectra on $In_{0.05}Al_{0.20}Ga_{0.75}N$. Energy values of excitation light correspond to band-to-band and inner-core excitation.

[1] K.Okada, K. Fukui, S. Naoe, S. Hamaura, H. Hirayama, Y. Aoyagi : UVSOR Activity Report 2002, 159 (2003).

BL1B

UV Spectroscopy on Condensed Oxygen under Pressure

Y. Akahama, T. Moriwaki and H. Kawamura
Department of Material Science, Graduate School of Science, Himeji Institute of Technology, Kamigohri, Hyogo 678-1297, Japan

Recently, metal-insulator transition has been reported in highly condensed oxygen. Many arguments have also been made on the formation of O_4 molecular in condensed phase up to now. In order to understand the phenomena from the electronic structure of molecules, the study of electronic spectra on condensed oxygen is indispensable.

Our recent studies on VUV absorption spectra of condensed oxygen up to 13 GPa have revealed that in super-critical fluid of oxygen, a relatively strong absorption band was observed in a UV region between 5 eV and 7 eV and the valence band of the β solid phase was developed from the new UV band. Therefore, the nature of the new band holds the key to clarify the phenomena. In this study, detailed absorption experiments have been carried out in a wide temperature range from 15K to 300 K.

Experimental

Liquid oxygen was loaded in the sample chamber of a sapphire-anvil pressure cells and pressure was regulated at 300 K based on a ruby pressure scale. The typical thickness and diameter of the sample chamber were about 46 μm and 250 μm, respectively. The UV absorption measurements were developed over a range from 0.2 to 1.5 GPa using VUV source at the BL-B1. Low temperature measurements were also carried out in a liquid-He spray-type cryostat.

Results and Discussion

Figure 1 shows the absorption spectra of condensed oxygen at pressures up to 1.5 GPa at 300 K. The spectra were measured using a sapphire anvil cell. The absorption spectra show a photon energy dependence of $(E-E_0)^{3/2}/E$ corresponding to a forbidden transition between a direct band gap, E_0, in a solid. From the dependence, E_0 was estimated to be 4.7 eV and independent on pressure. The coefficient: α for a photon energy of 5.5 eV increased linearly with increasing pressure. The absorption cross-section, which was estimated from the molar volume vs pressure relation recently obtained from our x-ray diffraction experiments, were consistent with the earlier data to 20 atm [1].

Figure 2 shows the temperature dependence of the spectra. With decreasing temperature, the sample pressure of 0.41 GPa at RT deceases to 0.1 GPa at 90 K. The sample transformed to the γ-O_2 solid phase with cooling to 80 K and the β-O_2 phase to 60 K and further to the α-O_2 phase at 30 K. The spectra reflect the pressure change as well as these phase transitions. We should note that a dumping of transmitting light occurred for the α-O_2 phase due to light-scattering at the crystal grains boundary.

One probable explanation of the nature for the new absorption band is that the Herzberg system of the $^3\Sigma_g^- \rightarrow {}^3\Sigma_u^+$ or $^3\Delta_u$, $^1\Sigma_u^-$ transitions becomes allowed as the result of an intermolecular interaction, though it is basically forbidden by parity selection rules. The formation of $(O_2)_2$ molecular units may be enable to allow the transition. The fact that two molecules transition was observed relatively strong in the α-O_2 phase, means that the true character of the dimer is an antiferromagnetic O_2 pair. The pair is stabilized with increasing pressure.

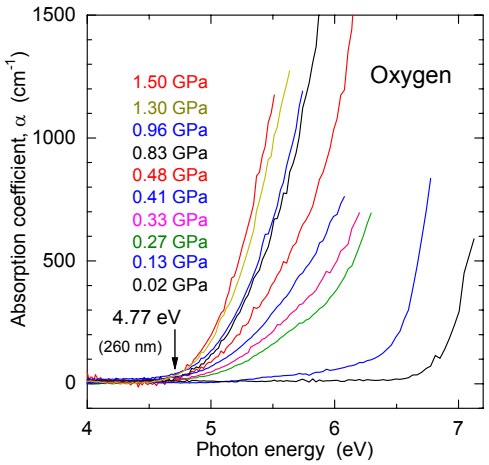

Fig.1 UV absorption spectra of condensed oxygen at various pressures at RT.

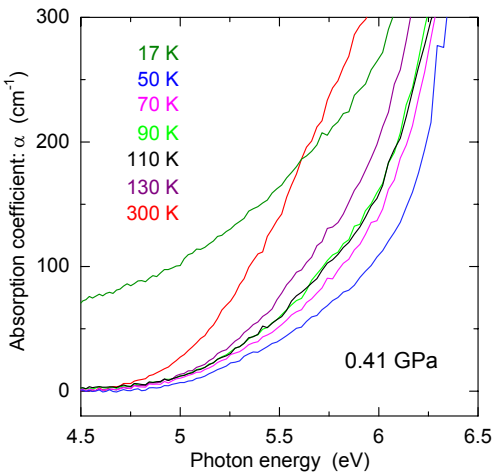

Fig. 2 UV absorption spectra of condensed oxygen at various temperatures. Sample pressure was 0.41 GPa at room temperature.

[1] Shardamand, Phys. Rev. **186**(1969)5.

BL-1B

Photoluminescence of Hydrogen-bonded Ferroelectrics CsH_2PO_4

T. Fuyuki, N. Ohno
K. Deguchi*

Division of Electronics and Applied Physics, Graduate School of Engineering
Osaka Electro-Communication University, Neyagawa, Osaka 572-8530, Japan.
** Shizuoka Institute of Science and Technology, Fukuroi, Shizuoka 437-8555, Japan.*

Cesium dihydrogen phosphate CsH_2PO_4 (CDP) is one of hydrogen-bonded ferroelectrics. CDP shows a first-order ferroelectrics phase transition from monoclinic $P2_1/m$ to orthorhombic $P2_1$ at $T_C = 156$ K. The PO_4^{3-} tetrahedra are linked to linear chains by hydrogen bonds along the *b*-axis, which is in contrast to well-known KH_2PO_4 (KDP) with the three-dimensional linkage of the hydrogen bonds.

The reflection and absorption spectra of CDP have been reported in the VUV region by our group [1]. The first reflection peak is observed at 10 eV. The spectrum near the fundamental absorption edge is quite similar to the previous results of KDP [2,3]. The absorption edge is located at 7.40 eV at 12 K. The temperature dependence of the absorption-edge energy was investigated in detail at around the T_C, showing an anomalous shift at T_C.

In the present study, photoluminescence and photo-excitation spectra of CDP have been investigated at the BL1B station. The optical measurements of KDP were also carried out for comparison. The specimens of CDP and KDP were grown at about 50°C by slow cooling of a saturated aqueous solution after several times of recrystallization.

Figure 1 shows the luminescence (left-hand side) and the excitation (right-hand side) spectra of CDP measured at 12 K. The luminescence spectrum was excited with 7.50 eV photons. Two luminescence bands are observed at 3.95 eV and 5.12 eV. The dash line in the figure is the absorption-edge spectrum at 12 K [1]. The 3.95 eV band is mainly induced at the excitation on the low-energy side of the absorption edge. On the other hand, the 5.12 eV band is stimulated with photons above the fundamental absorption edge. In the case of KDP, a single luminescence band is observed at 5.26 eV as shown in Fig. 2. The excitation spectrum of the 5.26 eV band of KDP is similar to that of the 5.12 eV band of CDP. These luminescence bands exhibits a Gaussian lineshape and a large Stokes shift, induced under the excitation into the fundamental absorption region. Thus, it is likely that these luminescence bands are intrinsic in origin.

The temperature dependence of the luminescence spectra was investigated for both materials. Unfortunately, these luminescence bands are found to be unstable at high temperatures; the luminescence bands are thermally quenched at ~ 80 K far below T_C.

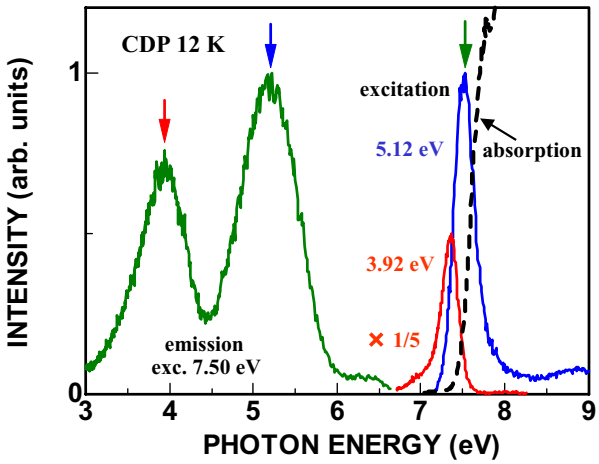

Fig. 1. Luminescence, excitation and absorption spectra of CDP at 12 K.

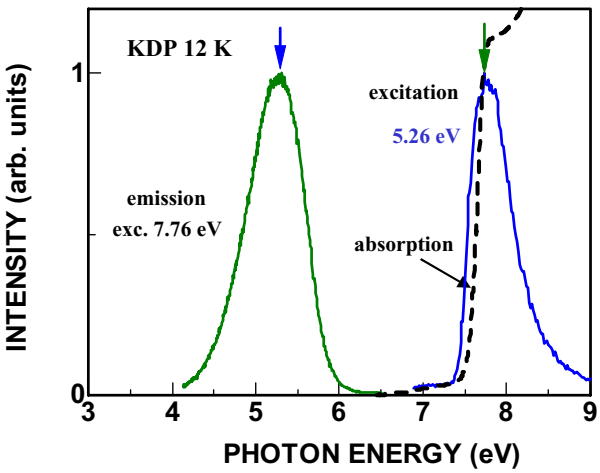

Fig. 2. Luminescence, excitation and absorption spectra of KDP at 12 K.

[1] T. Fuyuki, N. Ohno, K. Sasaki and K. Deguchi, UVSOR Activity Report 2002, **30** (2003) 106.
[2] S. Saito, K. Wada and R. Onaka, J. Phys. Soc. Jpn. , **37** (1974) 711.
[3] S. Matsumoto, M. Fujisawa and S. Suga, J. Electron Spectrosc. Relat. Phenom., **79** (1987) 615.

BL1B

Nonuniform Distribution of Adsorbed Dye at the Water Surface Probed by Photoionization Methods

T. Ishioka and A. Harata

Department of Molecular and Material Sciences, Kyushu University, Kasugakoen 6-1, Kasuga-shi, Fukuoka 816-8680, Japan

Photocurrent has been measured at a dye-adsorbed and hydrophobic-acid-modified water surface by synchrotron radiation and Nd:YAG laser irradiation. Photocurrent increase was observed when submonolayer amount of acid was added. It is suggested that the increased current is caused by aggregate formation of dye and acid molecules from large pulse-to-pulse fluctuation of photocurrent by laser two-photon ionization experiments.

SR light has a merit in measuring threshold energies by its inherent tunability in photon energy compared to lasers. However, it is hard to attain microscopic information at the water surface by SR because of the difficulties to focus the SR light to the μm level on the water surface by using conventional optics. If self-assembled or aggregated species are present at the water surface, local deviations should be large in photoionization intensities or threshold energies that are not observed in the conventional method.

A solute in a bulk solution is known to photoionize at a lower photon energy than the ionization potential in the gas phase due to neighboring solvent molecules. Lowering of the ionization threshold can also be observed in the case of adsorbed molecules at an aqueous solution surface though remarkable differences in energies are observed.[1] However, it is not clarified how a solute interacts on photoionization with its surrounding molecules in aggregated or self-assembled cases. Furthermore, formed surface structures might distort photoionization process itself because long alkyl chain or charged group can scatter electrons emitted by photoionization. In this study, photocurrent is measured of a water-soluble dye with an aliphatic acid that form surface-layer by single-photon ionization using SR and two-photon ionization using a Nd:YAG laser.

Experimental

The monochromated synchrotron light (4-8 eV) was obtained from BL1B at the UVSOR facility and emitted from the chamber to the He-purged cell through an MgF_2 window. The emitted light was reflected on an Al mirror and vertically irradiated on the aqueous solution surface through a Cu-mesh electrode. The electrode was set at 5 mm high above the liquid surface and high voltage (500 V) was applied. The photocurrent (~100 fA) was measured by a picoammeter. For two-photon ionization measurements, third-harmonic of a Nd:YAG laser was focused on the solution surface by a lens using the same cell and the transient photocurrent was amplified by a current amplifier. The signal was monitored by an oscilloscope.

The sample solutions were composed of surface-active dye (rhodamine B, 10 μM), a buffer electrolyte (HCl, pH 1.0), and water. The aqueous solution surface was modified with aliphatic acid (arachidic acid, $C_{19}C_{39}CO_2H$) by spreading as a benzene solution. The added amount was approximately within two monolayers at maximum that is calculated by the assumption that close-packed layer was formed on the aqueous solution surface.

Results and Discussion

Figure 1 shows the plot of the photocurrent against the added amount of arachidic acid measured by two-photon ionization. The current intensity remarkably increases when a small amount of acid is added and decreases to a constant value above monolayer formation level. These experimental results cannot be explained by a simple model that is described by the uniform monolayer formation and simple electron scattering through the aliphatic monolayer because this model needs monotonous decrease of photoionization current upon film formation. At the concentration range of increased photocurrent, it is found that pulse to pulse deviation is remarkably increased. The increased fluctuation suggests the presence of small domains that are comparable to the focused area (10-100 μm). From above results, aggregate formation and accumulation of dye molecules around the aggregate is a most probable explanation for the results.

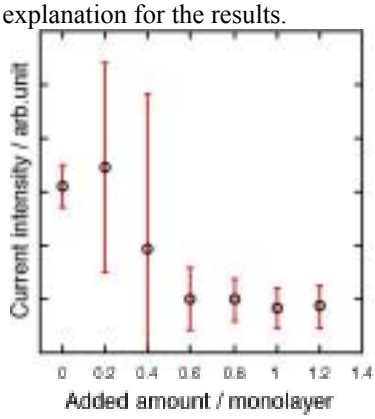

Fig. 1. Effect of arachidic acid addition on the photocurrent from the surface of rhodamineB aqueous solution by two-photon ionization. Bars indicate deviations of current intensities for each laser pulse.

[1] T. Ishioka, K. Seno, A. Harata, and Y. Hatano, *UVSOR Activity Report 2001*, 104.

[2] T. Ishioka, A. Harata, and Y. Hatano, *UVSOR Activity Report 2002*, 108.

BL1B

Effects of Additives and Photodegradation on the Photoluminescence in Polypropylene

T. Ito, N. Fuse, Y. Ohki

Department of Electrical Engineering and Bioscience, Waseda University, Shinjuku-ku, Tokyo 169-8555 Japan

Photoluminescence (PL) and photoluminescence excitation (PLE) spectra were observed in polypropylene (PP) by irradiation of photons from synchrotron radiation (SR) at 300 K. The samples, some of which are additive free and the rest contain additives, are named as listed in Table 1.

Fig. 1(a) shows the PL spectrum induced in the sample PN by the irradiation of SR photons at 5.8 eV and its three Gaussian-fitted curves. Therefore, the sample PN has three PL component bands around 4.2, 3.6, and 3.1 eV, which are hereafter referred to as A1, A2, and A3, respectively. Fig. 1(b) shows the PLE spectra in the sample PN detected at 4.1 and 3.6 eV. Since curves 1 and 2 in Fig. 1(b) can be reasonably assumed to reflect mainly PLs A1 and A2 respectively, their respective PLE peaks are found to be around 6.2 and 5.3 eV. Note that the PLE spectrum of PN detected at 3.1 eV could not be obtained clearly with a good reproducibility since the PL component at 3.1 eV is very small and is superposed with the component at 3.6 eV. Further experiments have shown that all the other PP samples PA, PB, PC, and PD have similar PL and PLE spectra. Therefore, we conclude that the additives in PP do not contribute to the PLs.

In order to examine the effects of photodegradation on the photoluminescence, all the samples were pre-irradiated by 6.4-eV photons from the ArF excimer laser either in vacuum, air, or in oxygen. Fig. 2 shows the PL spectra induced by the irradiation of 5.6-eV photons in the pre-irradiated PN sample. The PL components A1, A2, and A3 are decreased by the pre-irradiation, and a new PL component, referred to as PL B, with its center around 2.9 eV is induced. The intensity of PL B becomes larger when the oxygen pressure during the pre-irradiation is lower. Note that similar results were observed in all the other samples. This result indicates that the same PL B appears in all the samples by the UV pre-irradiation.

At least two candidates are possible as the chromophores for PLs A1, A2, and A3. The first candidate is the α, β-unsaturated carbonyl, which is commonly present in impurities in organic polymers. This carbonyl has the following structure,

$$-CH_2-CH=CH-C(=O)-CH_2-.$$

Namely, it has a pair of conjugated double bonds and is known to have a PL band around 4 eV, at an energy similar to PLs A1, A2, and A3. By the irradiation of UV photons, the α, β-unsaturated carbonyl becomes the β, γ-unsaturated carbonyl that has the following structure,

$$-CH=CH-CH_2-C(=O)-CH_2-.$$

Namely, the two double bonds in the β, γ-carbonyl are not conjugated, and are not luminous. This may explain the disappearance of PLs A1, A2, and A3 in the pre-irradiated polymers. The other candidate is a polynuclear aromatic impurity, which is commonly present in organic polymers. Polynuclear aromatics are known to have a PL band around 4 eV, of which intensity decreases if the sample is subjected to irradiation of UV photons.

Table 1. Samples Examined.

Name	Polymer	Additive
PN	PP	Free
PA	PP	AO
PB	PP	N
PC	PP	SA
PD	PP	AO, N, SA

(Note) AO: antioxidant; N: neutralizer; SA: slipping agent.

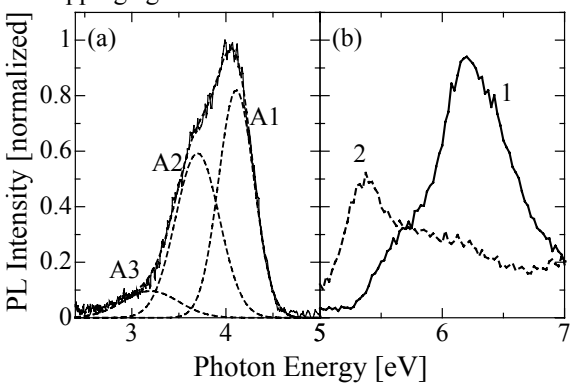

Fig. 1 (a) PL spectrum in the sample PN. (b) PLE spectra detected at 4.1 eV (curve 1) and 3.6 eV (curve 2) in the sample PN.

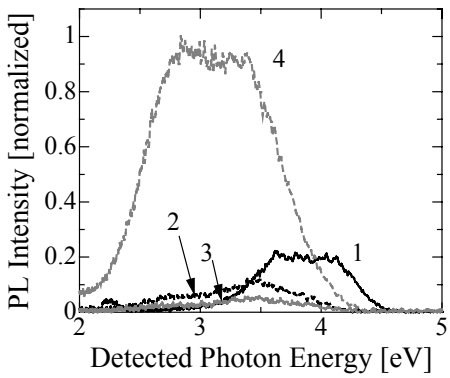

Fig. 2 Effects of pre-irradiation of UV photons in various atmospheres on PL spectra. Curve 1: as-received, 2: pre-irradiated in air, 3: pre-irradiated in oxygen, 4: pre-irradiated in vacuum.

BL1B

Optical Properties of Ammonium Chloride Doped with Tl^+ Ions

T. Kawai, S. Hashimoto

Department of Environmental Sciences, Faculty of Science, Osaka Women's University, Daisen- cho 2-1, Sakai City, Osaka 590- 0035, Japan

Ammonium halides are ionic crystals having the similar crystal and electronic structures as alkali halides. Since alkali halide crystals have played an important role as a host material for Tl^+- type ions such as Tl^+, Pb^{2+}, and Au^- [1], ammonium halide crystals are also an attractive host material for a number of Tl^+-type ions. However, the optical properties of the Tl^+ ions doped in ammonium halides are comparatively less studied, especially up to the vacuum ultraviolet energy region.

Single crystals of $NH_4Cl:Tl^+$ were grown from saturated aqueous solution containing various TlCl concentrations from 10^{-2} to 10^{-6} mole %. Urea was added into the solution as a habit modifier in order to obtain the good cube shaped samples. Optical measurements up to the vacuum ultraviolet energy region were performed at a BL-1B beam line of UVSOR. The samples were mounted on the cold stage of a flow- type cryostat and cooled down to 13 K. The light beam from the 750 MeV electron storage ring of the synchrotron radiation was monochromatized through a 1 m Seya- Namioka type monochromator. The luminescence and excitation spectra were measured by using an optical detection system composed of a grating monochromator (Jobin Yvon HR320) and a photomultiplier (Hamamatsu R955).

In the $NH_4Cl:Tl^+$ crystals, the A and C absorption bands due to the cationic transition in the Tl^+ ion are observed at 5.22 and 6.59 eV, respectively [2]. Under the excitation on the A absorption band at 13 K, the broad luminescence band peaking at 4.35 eV is dominantly observed. When the C absorption band at 6.59 eV is excited, the luminescence band peaking at 3.37 eV appears in addition to the 4.35 eV band, as shown in Fig. 1 (a). Fig. 1 (b) shows the excitation spectra for both the luminescence bands. The excitation spectra for the 3.37 and 4.35 eV luminescence bands exhibit no response above the energy region of the intrinsic exciton transition and the strong one on the A and C absorption bands. Since there is the response on the lowest A absorption band in the excitation spectra, the luminescence bands should be ascribed to the reverse transition of the A absorption: the radiative transition from the relaxed excited states of $^3P_1$ in the Tl^+ ion. The 4.35 and 3.37 eV luminescence bands would be interpreted as the radiative transitions from the two Jahn-Teller minima having the trigonal (X) and tetragonal (T) symmetry on the adiabatic potential energy surface, respectively, from the analogy with the A_X and A_T luminescence bands of the Tl^+ center doped in the cesium halides [3].

By the way, the cesium halide crystals doped with the Tl^+ center exhibit the luminescence bands due to the perturbed self- trapped exciton in the visible region, in addition to the A_X and A_T luminescence bands [3]. The causes have been ascribed to the ion arrangements around the Tl^+ ion [3]. That is to say, the Tl^+ ion doped in CsCl- type cesium halides is surrounded by the eight nearest halogen ions in the different way from the Tl^+ ion surrounded by the six nearest halogen ions in NaCl- type alkali halides. However, the Tl^+ center doped in ammonium chloride with the CsCl crystal structure exhibits no luminescence band due to the perturbed self-trapped exciton even under the excitation on the higher absorption bands. The characteristic features of the luminescence and excitation spectra of $NH_4Cl:Tl^+$ are similar to those of the Tl^+ center doped in the NaCl- type alkali halides. This fact indicates that the luminescence bands due to the perturbed self- trapped exciton are not induced by the eight nearest halogen ions around the Tl^+ ion.

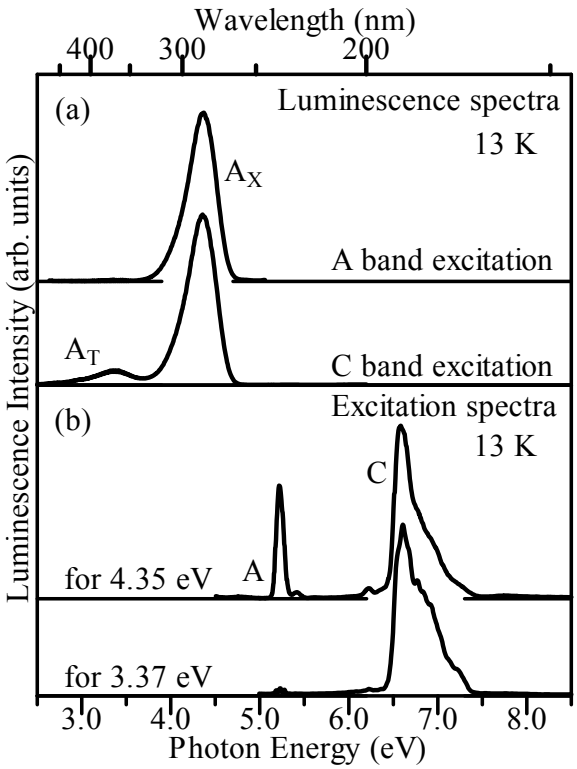

Fig.1. (a) Luminescence spectra
(b) Excitation spectra

[1] P. W. M. Jacobs: J. Phys. Chem. Solids **52** (1991) 35.
[2] T. Kawai and S. Hashimoto: J. Phys. Soc. Jpn. **21** (2002) 2566.
[3] S. Zazubovich, A. Voloshinovskii and G. Stryganyuk: phys. stat. sol. (b) **233** (2002) 238.

BL1B

Vacuum-ultraviolet Reflectance Spectroscopy of Transition-metal Oxides and Chalcogenides

M. Matsubara[1], S. Miyasaka[1], Y. Shimada[1], and Y. Tokura[1,2,3]

[1] *Department of Applied Physics, University of Tokyo, Tokyo 113-8656*

[2] *Correlated Electron Research Center (CERC), National Institute of Advanced Industrial Science and Technology (AIST), Tsukuba 305-8562*

[3] *Spin Superstructure Project, ERATO, Japan Science and Technology Corporation (JST), Tsukuba 305-8562*

One of the most important characteristics for the correlated electron systems is the drastic re-construction of electronic structure over an energy scale of eV with changes of temperature, doping concentration, and/or external field. Therefore, optical reflectivity measurement over a wide energy range and the optical conductivity spectra derived from the reflectivity spectra provide us with very useful information about the strongly correlated electron systems.

In this beam time, we measured the reflectivity spectra of several transition-metal oxides and chalcogenides, including V, Cr, Mn, Fe and Mo, for an energy range of 4 eV < E < 35 eV at room temperature using the beam line BL1B. The measured reflectivity data, together with the lower-energy data below 6 eV, were used to derive the optical conductivity spectra or dielectric function via the Kramers-Kronig analysis. As an example, the imaginary part of the dielectric function of a single crystal of $GaFeO_3$, which is grown by a floating zone method, is shown below.

$GaFeO_3$ is a prototypical polar ferrimagnet and shows magneto-electric effect at low temperatures. The absorption bands indicated as A and B correspond to transitions from O 2*p* to Fe *3d* state and the bands denoted as C and D are due to the transition between O 2*p* and Ga *4s* levels. This system has two sites of Fe and Ga. The different sites of Fe and Ga may cause the splitting (A and B, C and D). The structure indicated as E corresponds to the transition from O 2*s* to Fe 3*d* state.

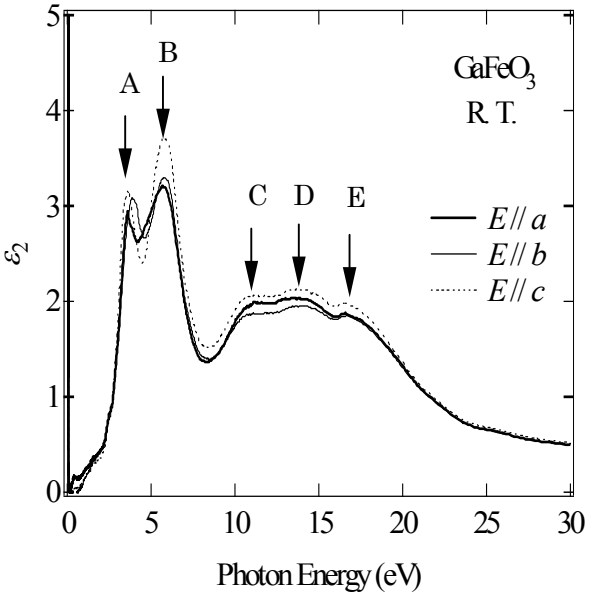

Figure. Imaginary part of dielectric function for polarization configurations of *E//a*-, *b*- and *c*-axis in $GaFeO_3$.

BL1B

Reflection Spectrum and Auger-Free Luminescence in Cs_2ZnCl_4

A. Ohnishi, M. Kitaura* and M. Sasaki

Department of Physics, Faculty of Science, Yamagata University, Yamagata 990-8560 Japan

** Fukui National College of Technology, Geshi, Sabae 916-8507 Japan*

Cs_2ZnCl_4 is orthorhombic and belongs to *Pnam* space group. In this material, thermo-chemical properties, dielectric properties and so on have been studied [1,2]. As for optical properties, however, there are only a few reports on absorption and emission spectra in the infrared region of a Cs_2ZnCl_4: Co^{2+} [3]. In this paper, we report the observation of the Auger free (AF) luminescence emitted from Cs_2ZnCl_4, in addition to that of the fundamental absorption.

Cs_2ZnCl_4 crystals were prepared by evaporating a stoichiometric mixture of solutions of CsCl and $ZnCl_2$. Experiments were performed at the BL1B of UVSOR equipped with a 1-m Seya-Namioka VUV monochromator. Reflection spectra were measured with a photomultiplier (Hamamatsu R105) coated by sodium salycilate phosphor. Luminescence from the sample was measured using a quartz lens, a grating monochromator (Jobin Yvon HR 320) and a photomultiplier (Hamamatsu R955).

Figure 1 shows the reflection spectrum of Cs_2ZnCl_4 at 10 K. Sharp bands are observed at 7.15, 7.67 and 8.78 eV. We tentatively assign the 7.15 eV band to the n = 1 exciton absorption, which is due to the transition from the Cl 3*p* valence band (VB) to the Cs 6*s* conduction band (CB) on the basis of the calculation of the electronic state for a $[Cs_3ZnCl_4]$ cluster with the DV-Xα method. In the range of 13−14 eV, some weak peaks are observed. The transition energy of 13 eV is in almost agreement with the sum of the band gap energy E_g = 7.95 eV and the energy difference E_{vc} = 5.0 eV between the top of VB and that of the outermost core band. Thus, the peaks are attributed to the transitions from the core level to the conduction band.

It should be noticed that E_g is larger than E_{vc} in Cs_2ZnCl_4. This suggests the possibility that the AF luminescence is observable in this material. Figure 2 shows the emission spectrum observed at room temperature (RT) under excitation with 14.0 eV light. An intense luminescence band appears at 4.15 eV, along with a weak band at 3.31 eV.

In Fig. 3, the excitation spectrum for the 4.15 eV band is plotted. The excitation spectrum for the 3.31 eV band was practically the same as that for the 4.15 eV band. The spectrum rises from the energy position around 13 eV, and the intensity is almost constant in the range of 16−22 eV and increases above around 23 eV. It is noteworthy that the observed threshold energy corresponds to the onset of the transition between the outermost core level and the conduction band. On the basis of this, we suppose that both of the 4.15 eV and 3.31 eV bands come from the radiative recombination between the valence electron and the outermost core hole.

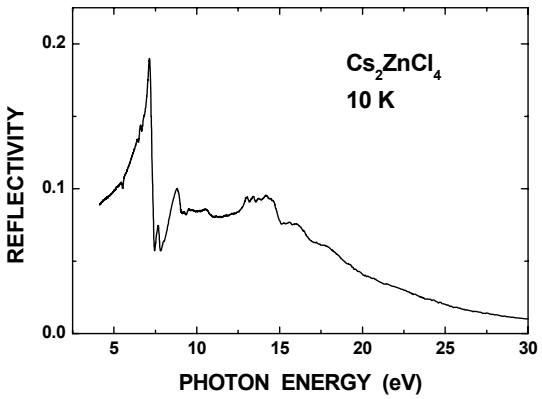

Fig. 1

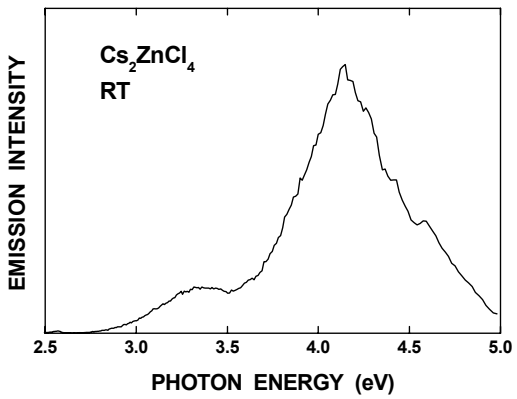

Fig. 2

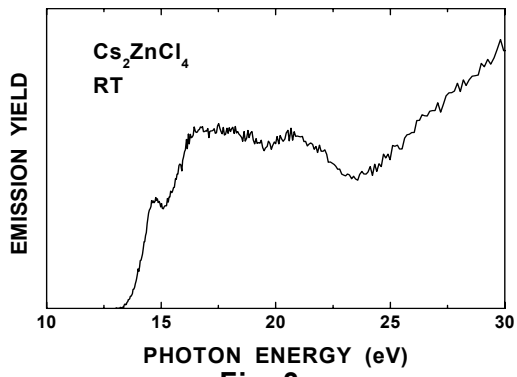

Fig. 3

[1] F. Ying, L. Liangchao and Q. Songsheng: Thermochimica Acta **303** (1997) 187.

[2] A. Onodera, O. Watanabe, H. Haga, K. Kikuta, E. Suzuki, H. Yamashita and Y. Shiozaki: Ferroelectrics **125** (1992) 141.

[3] P. J. Deren, J. Derouet, P. Porcher and D. Svoronos: J. Mol. Struct. **404** (1997) 167.

BL1B

Superlattice Structure and Optical Spectroscopy of $SrMgF_4:Ce^{3+}$ Crystals

M. Yamaga[1], K. Itoh[1], S. Yabashi[1], Y. Masui[1], S. Ono[2], M. Sakai[2], and N. Sarukura[2]

[1]*Department of Electric and Electronic Engineering, Gifu University, Gifu 501-1193, Japan*

[2]*Institute for Molecular Science, Okazaki 444-8585, Japan*

Laser action was reported on interconfigurational transitions in $LiYF_4:Ce^{3+}$ and $LiCaAlF_6:Ce^{3+}$. However, it has not been achieved for other fluorides crystals in spite of their high energy band gaps. We reported VUV spectroscopy of CaF_2 codoped with Ce^{3+} and Li^+/Na^+ at low temperature[1]. As Ce^{3+} substitutes for Ca^{2+} in CaF_2, charge compensators, for example, Li^+/Na^+ ions are required. It was found from the VUV spectra that several Ce^{3+} centers are perturbed by the charge compensators located at different nearest neighbors.

We have grown $SrMgF_4$ crystals doped with Ce^{3+} as a new laser material using the Bridgmann -Stockbarger method. The x-ray diffraction analyses for the $SrMgF_4:Ce^{3+}$ crystals indicate the existence of superlattice structure. As the superlattice structure has several different Sr^{2+} lattice sites which are replaced by Ce^{3+}, it is expected to perform wider tuning. In this report, the relation between optical properties of various Ce^{3+} centers and the superlattice structure is discussed.

The optical absorption spectrum of the $SrMgF_4:Ce^{3+}$ crystals in VUV range measured at 15 K is shown at the top of Fig. 1. There are several broadbands with peaks at 1400, 1500, 1800, 2200, 2500 and 2750 Å in the VUV and UV ranges.

The 140-nm VUV excitation produces two different luminescence bands with double peaks at (21500, 23500 cm^{-1}) and (24500, 26500 cm^{-1}), respectively, denoted by A and B. The 205-nm and 217-nm UV excitations produce different luminescence bands with double peaks at (30000, 32000 cm^{-1}) and (31500, 33500 cm^{-1}), respectively, denoted by C and D. The excitation spectrum of the A-band luminescence consists of two intense bands at 1800 and 2000 Å and weak three bands at 2500, 3150, 3800 Å. Similarly, the excitation spectra of the B, C and D luminescence bands are shown in Fig.1. Remarkable features of these luminescence and excitation spectra are as follow as.

(1) The luminescence spectra of A, B, C and D consist of two broadbands with separation energies of about 2000 cm^{-1}.

(2) The excitation spectrum of the A bands with lower energy peaks spread from 1700 to 3800 Å. On the other hand, the excitation spectrum of the D bands with higher energy is composed of five bands located at narrow range of 1500-2500 Å.

These results suggest relation between the superlattice structure of $SrMgF_4$ and crystal field of Ce^{3+}. The x-ray diffraction analyses show four different polyhedra of Sr coordinated with nine, ten and eleven fluoride ions. The large number of coordination may correspond to the large crystal filed splitting, resulting in red shift of the Ce^{3+} luminescence. Then, in the order of D, C, B and A , the crystal field splitting becomes small.

[1] M. Yamaga, S. Yabashi, Y. Masui, M. Honda, H. Takahashi, M. Sakai, N. Sarukura, J.-P.R. Wells, and G.D. Jones, J. Lumin. (2004) in press.

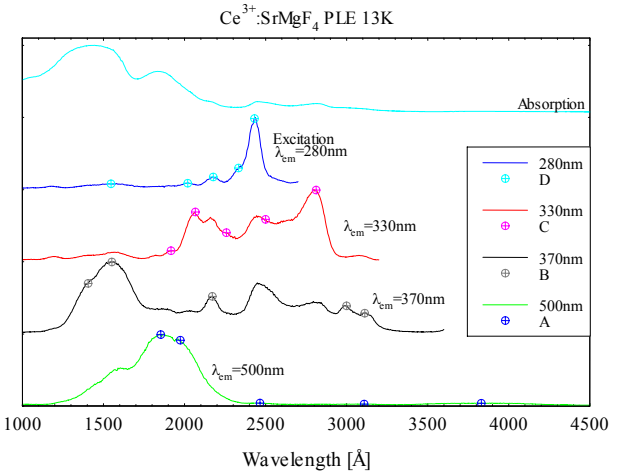

Fig.1 Absorption and excitation spectra of Ce^{3+} in $SrMgF_4$

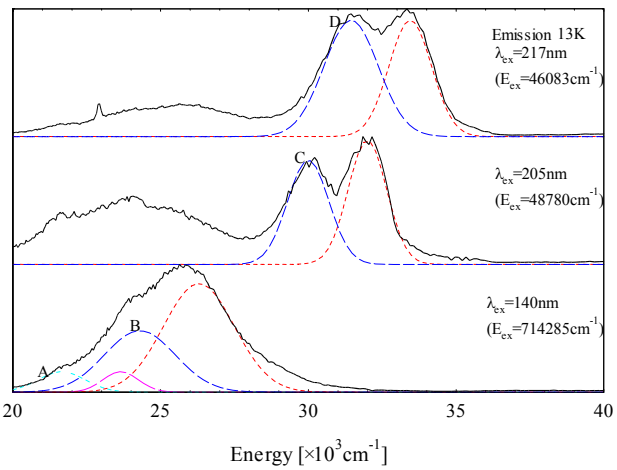

Fig.2 Luminescence spectra of Ce^{3+} in $SrMgF_4$

BL5B

The Measurement of the Transmission Spectrum of an Amorphous Semiconductor Thin Film

K. Hayashi

Department of Electrical and Electronic Engineering, Gifu University, Gifu 501-1193, Japan

It is well known that amorphous semiconductor materials are very sensitive to the light and show a variety of photoinduced phenomena [1,2]. Therefore, amorphous semiconductor are very much expected as materials for optoelectronic devices, such as solar cells, thin film transistors, light sensors, and optical memory devices etc. These applications require an understanding of the physical properties of amorphous materials. In our recent study, we observed interesting photoinduced change in the photoconductivity and the total photoyield of amorphous chalcogenide films by the irradiation of the vacuum ultraviolet (VUV) light and the visible light with the energy corresponding to the optical bandgap [3]. To obtain a wide knowledge of the photoinduced phenomena, we investigated photoinduced effects in the VUV region by the reflection spectra. However the signal-to-noise ratio is not good in some cases in the reflection spectrum measurement. In present report, measuring method of the transmission spectrum was examined.

It is possible that the amorphous semiconductor sample for the measurement of the transmission spectrum easily makes a thin film by conventional evaporation technique. The ultrathin collodion film was used as a substrate for the measurement of the transmission spectrum. The ultrathin collodion films were prepared onto metal plates with a pinhole of the diameter of 1.5mm. The transmission spectrum was measured through this pinhole. The metal thin films are often used in order to eliminate the higher order light from the monochromator in the VUV region. It is important to investigate the annealing effects, when the photoinduced phenomena in the amorphous materials are studied. It can be used as a higher order light cutoff filter in the VUV region, and as a possible heat-treating substrate, a metal thin film is more useful than collodion film. At present, the transmission spectrum of amorphous materials has mainly planned the measurement in the wavelength region between 20nm and 35nm. An aluminum thin film is useful as a substrate, because it can be used as higher order cutoff filter in this wavelength region. In this report, the following was examined: optimum film thickness and performance as higher order light cutoff filter.

Aluminum thin films were prepared onto substrates of ultrathin collodion films by conventional evaporation technique. The film thickness was controlled by the filling quantity of the source material and the deposition time as a convenient method. The measurement of the transmission spectra in the VUV region was performed at room temperature at the BL5B beam line of the UVSOR facility of the Institute for Molecular Science.

Figure 1 shows the VUV transmission spectra in aluminum thin films with the different film thickness. The transmission spectrum of a commercial aluminum filter with 100nm film thickness supported by the metal mesh is also shown in Fig.1. In the figure, every transmission spectrum has not been normalized by the spectroscopic system response, and they have been normalized at the maximum value of the transmitted light strength. As can be seen in the figure, features of the spectrum observed in each aluminum film agree well to each other. In addition, the filter character that is equivalent to the commercial filter has been obtained in the prepared thin film. From present result, it is concluded that the aluminum thin film filter can be easily manufactured. The aluminum thin films will be used as substrates, and the amorphous semiconductor thin films are prepared onto them, and the transmission spectrum will be measured.

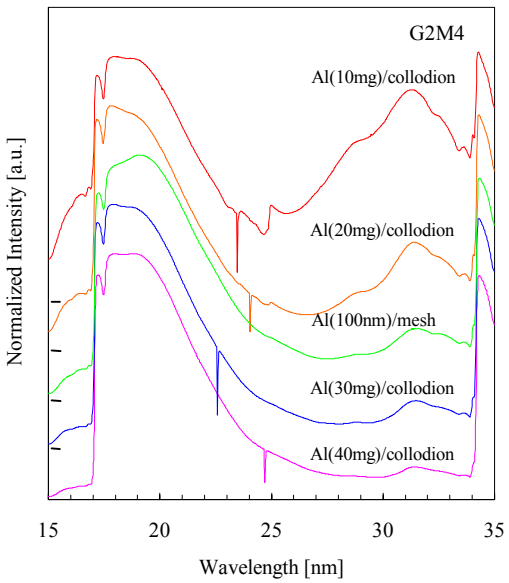

Fig. 1. Normalized transmission spectra of Al/collodion and Al/mesh.

[1] Ke. Tanaka, Rev. Solid State Sci., 4(1990)641.
[2] K. Shimakawa, A. Kolobov, and S. R. Elliott, Adv. Phys., 44(1995)475.
[3] K. Hayashi, A. Hirai, and K. Shimakawa, UVSOR Activity Report 1996(1997)116.

BL5B

L-shell NEXAFS of Sulfur in amino acids: Cysteine and Methionine

F. Kaneko[1*], K. Nakagawa[2], T. Kitada[1], A. Kasahara[1]

[1]*Graduate School of Human Science and Cultural Studies, Kobe University, Kobe 657-8501 Japan*

[2]*Faculty of Human Development, Kobe University, Kobe 657-8501 Japan*

** fusae@radix..h.kobe-u.ac.jp*

Using the upgraded UVSOR (UVSOR II), we measured L-shell NEXAFS of thin films of sulfur in metionine (Met, Fig. 1(A)) and cysteine (Cys, Fig. 1(B)), in an attempt to study the role of sulfur, the heaviest element in amino acids.

Cysteine and methionine powder was purchased from the Sigma Co. and used without further purification. These amino acids were evaporated carefully on BeCu substrates covered with 30nm Au. Thickness of sublimated amino acid films was measured by quarz oscillator to be 20nm and 150nm each other. Measurement was performed at BL-5B in energy region from 150eV to 270eV with the grating 2 and mirror 1. Wavelength resolution with the slit width of 0.05 mm was estimated to be 0.01nm from the half width of the 0-th order light spectrum.

We measured absorption spectra $A(\lambda)$ from the drain current $i(\lambda)$ divided by incident intensity I_0 (λ) monitored as drain current on Au mesh ($A(\lambda)= i(\lambda)/ I_0$ (λ)). All measurements were carried out at 300 K. Typical drain current was 50 pA at 200 eV with 200 mA SR ring current. Obtained spectra are shown in Fig. 2, in which background signal due to other atoms was subtracted by linear extrapolation and only L-shell component was shown. Mass absorption coefficient was estimated by normalizing the intensity at 160 eV and 235 eV by Henke formula [1]. In the figure, photon energy was not calibrated.

According to the X-ray data booklet [2], L_1, L_2 and L_3 levels of sulfur is known to be at 230.9, 163.6 and 162.5 eV, respectively. Thus we concluded that peaks at 226.0 eV for Met and at 226.9 eV for Cys are due to L_1 transition. Doublet peaks at 163.8 eV and 164.6 eV for Met and peaks at 163.6 and 165.0 eV were ascribed to L_2 and L_3 transition which showed the clear spin-orbit splitting. It should be noted that sharp peak was observed at 166.6 eV for Met. The origin of this peak is not clear now. Quantum mechanical calculation is being planned.

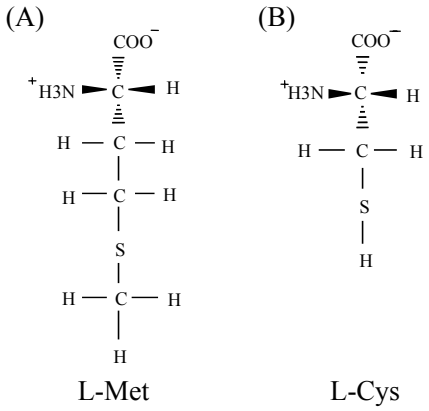

Fig.1. L-Methionine(A)andL-Cysteine(B).

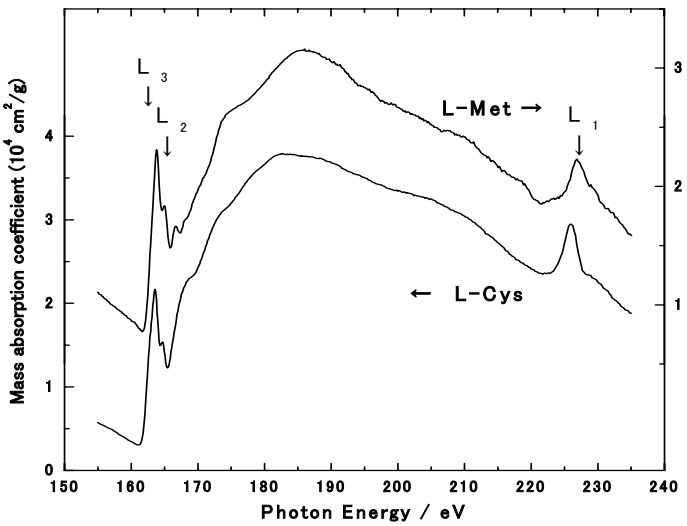

Fig. 2. L-shell NEXAFS of Sulfur in L-Methionine and L-Cysteine.

References

[1] B.L. Henke, E.M. Gullikson, and J.C. Davis, Atomic Data and Nuclear Data Tables Vol. **54** (no.2), 181-342 (July 1993).

[2] A. Thompson et al., "X-RAY DATA BOOKLET", ALS, 2001, p. 1-2.

BL5B

Characterization of Freestanding Metal Optical Filters and GaN UV Detectors in VUV and SX Region

A. Motogaito[1], H. Watanabe[1], K. Hiramatsu[1]
K. Fukui[2], Y. Hamamura[3], K. Tadatomo[4]
[1]*Dept. of Electrical and Electronic Engineering, Mie University, Tsu 514-8507 Japan*
[2]*Research Center for Development for Far-Infrared region, Fukui University, Fukui 910-8507 Japan* [3]*Core Technology Center, Nikon Corporation, Sagamihara 228-0828 Japan*
[4]*LED Business Development Dept., Mitsubishi Cable Co. Ltd., Itami 664-0027 Japan*

The characterization of freestanding thin film filters and GaN based Schottky ultraviolet (UV) detectors were carried out from vacuum ultraviolet (VUV) to soft X-ray (SX) region (25-100 eV, 12.4-50 nm). The high order light from grating of monochrometer was able to be eliminated by using Ti, Ti/Al/Ti and SiN thin films as a filter. Moreover, the transmittance of Schottky electrode Ni/Au calculated from that of Ti/Au membrane was about 50-70% in this wavelength region, and it is enough thin to transmit VUV and SX light. Measured using such a filter and transparent electrode, this detector can also detect VUV and SX light. The responsivity in VUV (30-50 nm) and SX region (@13 nm) was about 0.01 and 0.05 A/W, respectively.

UV detectors are one of the most attractive devices in the group III-nitride semiconductors. Currently, for the measurements of UV light, Si based photodiodes are mainly used. However, light sensitivity often deteriorates due to radiation damage in the vacuum ultraviolet (VUV) and soft X-ray (SX) region. To overcome this problem, several groups have reported on GaN- or AlGaN-based UV detectors such as photoconductor, the Schottky type, the Schottky-based metal-semiconductor-metal type, p-n or p-i-n type have been reported. However there are few reports for responsivity spectra in VUV and SX region [1].

On the other hand, there are few effective optical filters to remove higher order light generated by monochrometer in VUV and SX region. Thus it is important to develop effective optical filters in VUV and SX region.

In this report, the characterization of optical filters by using membranes and GaN UV detectors are characterized in BL5B and comparing the results of simulation data.

The details of fabrication of optical filters and GaN UV detectors have already reported [1].

The optical characterization of SiN and Ti/Al/Ti are carried out. The experimental data and theoretical data are almost agreed. Thus, from these results, the measurement of UV detectors is able to in the range between 37 and 100 eV. The transmittance of Ni/Au electrode is about 0.5-0.7 in this measurement range [2].

Using these filters, the responsivity spectra of GaN UV detectors are carried out. Figure 1 shows the responsivity spectra of GaN UV detectors between near UV and SX region. No responsivity at the energy lower than 3.4 eV can be observed clearly. The ratio of responsivity between UV and visible (VIS) regions is about 5×10^3. The maximum responsivity of this detector is about 0.10 A/W at $h\nu$=3.5 eV. The responsivity in VUV region (10-50 eV) is about 0.01 A/W. The larger responsivity is found in VUV-SX region (>50 eV). The value of responsivity in SX region (@13 nm for EUV lithography system) is about 0.05 A/W. To consider the reason of increasing responsivity between VUV and SX region (50-100 eV), the transmittance spectra of Ni/Au Schottky electrode and penetration depth of GaN for VUV and SX light are evaluated. Above 50 eV, the transmittance of Ni/Au electrode and the penetration depth of GaN are increasing with photon energy. Therefore, the larger responsivity is obtained in SX region compared to VUV region.

[1] A. Motogaito et al., Phys. Stat. Sol (a) 200 (2003) 147.
[2] A. Motogaito et al., UVSOR ACTIVITY REPORT 2002 (2003) 132.

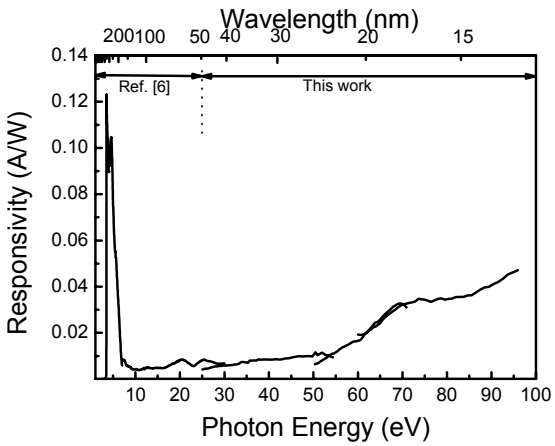

Fig. 1 The responsivity spectra of GaN UV detectors using SiN and Ti/Al/Ti optical filters in SX and VUV region.

BL5B

Wide-Range Reflection Multilayer in 200-25nm Region

T. Ejima, A. Yamazaki, T. Banse, M. Watanabe
IMRAM, Tohoku University, Sendai, 980-8577 Japan

A new high reflectance mirror for normal incidence in wide wavelength region (200-25 nm) is designed and fabricated. Reflectance of the fabricated mirror in 5° of angle of incidence is comparable with that of Pt in 200-35 nm region, is higher than any materials in 35-25 nm region.

Introduction

The working wavelength range of normal incidence optical systems has been limited above 40 nm, because normal incidence reflectances of usual mirror-materials are small below 40 nm. Therefore, the development of multilayers to extend the working range to shorter wavelength region has been made [1]. In this study, the efforts were made to extend the short wavelength limit from 40 nm to 25 nm, and new high reflectance mirrors in this region are designed and fabricated.

Design

A conceptual structure of the wide-range multilayer is given in Fig. 1. It is composed of a top-single-layer (TSL) reflecting light in 200-65 nm region, a middle-aperiodic-layers (MAL) reflecting light in 65-25 nm region, and a bottom piled-double-layers (PDL) reflecting light around 25 nm.

The wide-range multilayers were designed as follows [2]. At first, the bottom PDL is designed to enhance the reflectance around 25 nm. At second, a material and its thickness of a TSL are chosen to have a high reflectance in the 200-50 nm range. Finally, an MAL is inserted between the PDL and the TSL to make the reflectance flat in 85-25 nm region.

One of the multilayer structure is a PDL of Mg 9.0 nm/Y_2O_3 4.8 nm with 14 periods, a MAL of Mg 12.6 nm/Y_2O_3 5.0 nm, and a TSL of SiC 5.0 nm.

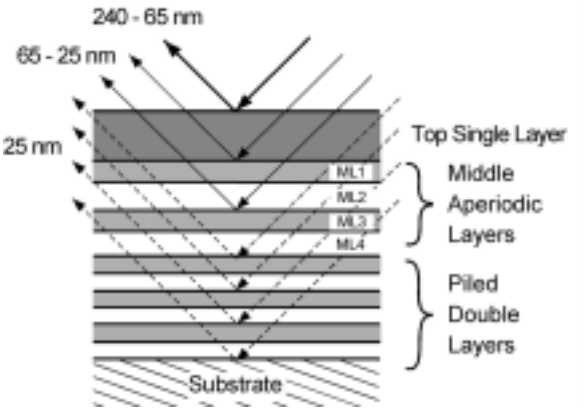

Fig. 1: Layer structure of the wide-range multilayer.

Experimental Results

Measured reflectance of the fabricated multilayer in 5° of angle of incidence is compared with the usual mirror materials in Fig. 2 (a). Measured reflectance of the multilayer is designated as the red curve, simulated reflectances of the materials are as the black curves. As can be seen in the figure, the measured reflectance of the fabricated multilayer is comparable with that of Pt in 200-35 nm region and is higher than any materials in 35-25 nm region.

Measured reflectance is also compared with the simulation results of the designed multilayer in Fig. 2 (b). The measured reflectance is lower than that of simulation in 200-62 nm region. This suggests that the fabricated thickness of the TSL, SiC, layer is thinner than the designed one. The reflectance in 62-41 nm and 31-23 nm regions is comparable with the simulation. These results suggest that the layer structure of the fabricated PDL fulfills the designed one. The lower reflectance in 41-31 nm region will be caused by the difference of the optical constants between the fabricated Y_2O_3 layer in MAL and the handbook data used in the simulations [3], because the Y-N absorption edge cannot be observed in the fabricated multilayer.

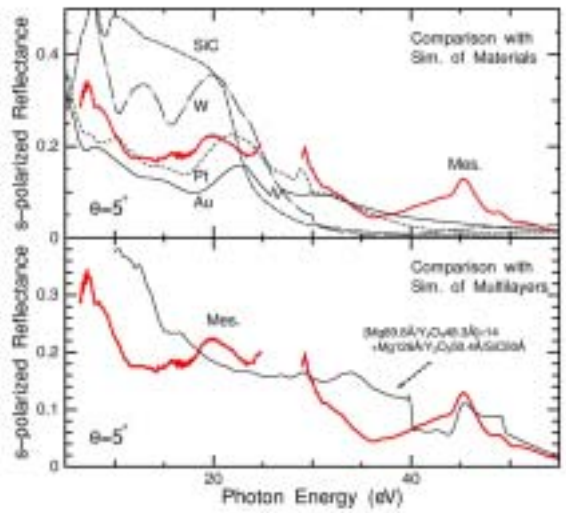

Fig. 2: Measured reflectance of the wide-range multilayer with simulations.

References

[1] Y. Kondo, T. Ejima, K. Saito, T. Hatano, and M. Watanabe, Nucl. Inst. Meth. Phys. Res. A **467-468** (2001) 333.

[2] T. Ejima, K. Sudo, T. Hatano, and M. Watanabe, J. Phys. IV France, **104** (2003) 259.

[3] *Handbook of Optical Constants of Solids II*, Ed. by Edward D. Palik, Academic Press, Inc., 1991.

BL5B

EUV Deterioration of Thin Filters

T. Murachi, K. Okada, M. Kanao, S. Kameda, H. Sagawa, and I. Yoshikawa
Institute of Space and Astronautical Science, Japan Aerospace Exploration Agency, Sagamihara, Kanagawa 229-8510 Japan

When the satellites keep up observation in long term, the deterioration of observational equipments becomes important problem [1], [2]. It is indispensable for analyzing data to investigate the deterioration of equipments. Especially we should know the changes of the equipments' extreme-ultraviolet-region performance by the deterioration because our equipments have observed with the extreme ultraviolet (EUV) light. Therefore, we produce the samples simulated the deterioration in the Space, and investigate that.

It is said that main causes of deterioration in the Space is solar high-energy particles and solar ultraviolet (EUV) ray. We can list the deteriorative equipments as follows: Mirror, MicroChannel Plates, Filters, and Black paint inside the hood. This time, we simulate the solar EUV deterioration of Filters by the intense light of UVSOR BL5B (PGM 35). And we investigate changes of their transmittance.

We irradiated the light (radius: ~ 1 mm) of 20 ~ 100 nm to the filter (radius: ~ 5 mm), which consists of half area of Carbon/Aluminum (thickness: 368/1429 Å) and another half area of Al (thickness: 1429 Å) as Fig. 1. The 1st order light of 30.4 nm was irradiated to the place of ~ 2 mm (C/Al area) from edge of C/Al, and 0th order light (20 ~ 100 nm) was irradiated to ~ 4 mm (C/Al area) and ~ 8 mm (Al area). In case of 0th order, irradiated quantity of light is ~ 6.5 × 10^{-2} J/mm^2 (Irradiated at ~ 3.1 × 10^{11} photons/sec/mm^2 in 9 hours. Energy of 0th order light calculates as 30.4nm (~ 6.6 × 10^{-18} J/photon).), and in case of 1st order, that is ~ 2.2 × 10^{-4} J/mm^2 (~ 3.1 × 10^9 photons/sec/mm^2 in 3 hours.). As the solar He II (30.4nm) flux is ~ 2 × 10^{-9} W/mm^2, ~ 6.5 × 10^{-2} J/mm^2 is approximately 2 week amount.

After irradiation, the filter becomes as Fig. 1. The part of the C/Al filter where 0th order light was irradiated changes from brown to black.

Fig. 2 is the measurement result of filter transmittance before and after EUV irradiation. Transmittance was measured in every 1 mm from the edge of C/Al to the edge of Al by the lights (30.4nm, 46.2nm and 58.4nm) of radius: ~ 1 mm. Values of irradiated place (list above) are consistent with each values of horizontal axis. The transmittance of black place (~ 4 mm, C/Al area) irradiated 0th order light has decreased remarkably. At 30.4nm transmittance is reduced from 12.5 % to 4.6 %, at 46.2nm from 1.8% to 0.16 %, and at 58.4nm from 0.24 % to 0.056 %. Such decrease is not seen in Al area. We think this decrease is caused by structure change of carbon filter because carbon layer was heated in the vacuum.

We understand that intense light should not shine in the carbon filter. For example, in condensing optics filters are not arranged in focus.

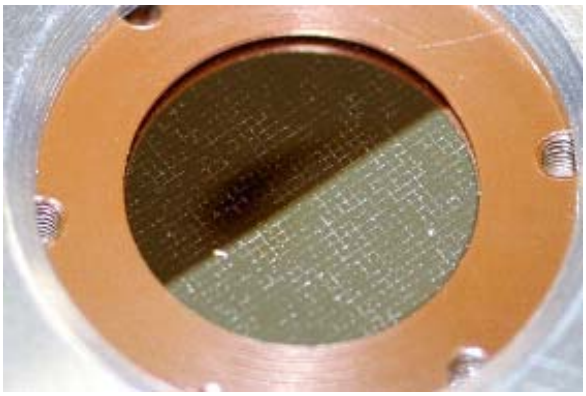

Fig. 1. The photograph of filter irradiated EUV. Upper brown half area is C/Al filter, and lower silver half area is Al filter. The black part in C/Al filter is where 0th light was irradiated.

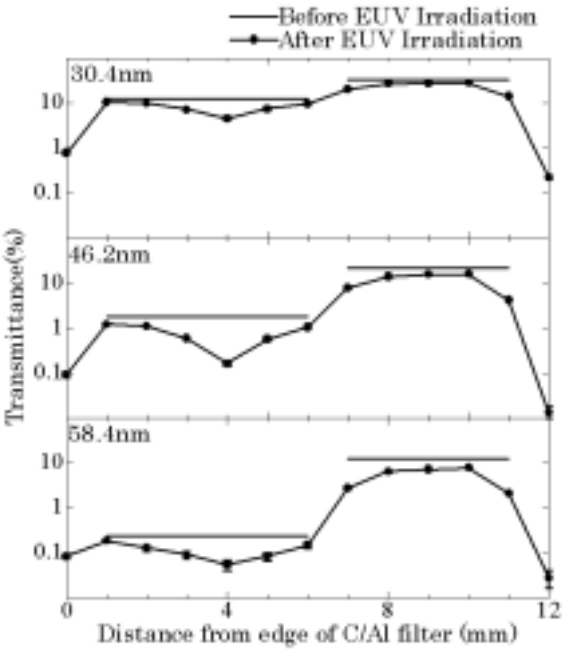

Fig. 2. Transmittance of filter before and after EUV irradiation. Measured wavelength is 30.4nm in top graph, 46.2nm in middle and 58.4nm in bottom. Horizontal axis represents distance (mm) from C/Al filter edge, and vertical represents transmittance (%).

[1] P. W. Vedder, J. V. Vallerga, J. L. Gibson, J. Stock, and O. H. W. Siegmund: Proc. SPIE **1742** (1992) 486.
[2] J. V. Vallerga, B. A. Roberts, J. Dupuis, and P. N. Jelinsky: Proc. SPIE **3356** (1998) 1001.

BL6A1

Millimeter Wave Reflection Measurements of Secondary Battery Substance $LiMn_2O_4$

H. Ohta, H. Ishikawa[A], T. Hirano[A], Y. Nagasaka[A], T. Nanba[A], A. Hirano[B] and R. Kanno[C]

Molecular Photoscience Research Center, Kobe University, 1-1 Rokkodai, Nada, Kobe 657-8501

[A]The Graduate School of Science and Technology, Kobe University, 1-1 Rokkodai, Nada, Kobe 657-8501

[B]Faculty of Engineering, Mie University, 1515 Kamihama-cho, Tsu 514-8507

[C]Interdisciplinary Graduate School of Science and Engineering, Tokyo Institute of technology, 4259 Nagatsuda, Midori, Yokohama 226-8502

As $LiCoO_2$ and $LiNiO_2$, which are in commercial use and a promising material for the Li ion secondary batteries, respectively, have attracted much attention recently, we have been studying the millimeter wave reflection measurements of these substances and related substances using UVSOR to investigate the dynamical properties of Li ions [1-9]. The increase of reflection is observed in the low energy region above 300 K for $LiNiO_2$ and $Li_{1-x}CoO_2$, and we proposed that this increase of reflection is related to the motion of Li ion in the system. However, it turned out to be flat in the observed region for $LiCoO_2$ [8]. The investigation to clarify the relation between the reflection and the charge-discharge process is under progress. On the other hand, $LiMn_2O_4$ is considered as a new promising material for the positive electrode of the Li ion secondary battery from the economical point of view. Therefore, we made a reflection measurements of $LiMn_2O_4$.

The reflection measurements of $LiMn_2O_4$ sintered sample with a diameter of 10 mm have been performed in the spectra region from 5 to 60 cm^{-1} using the beam line BL6A1 of UVSOR. The low pass filter was used for the measurement below 22 cm^{-1}. The temperature was changed from 77 to 380 K. The gold plate was used as a reference and InSb detector was used as a detector.

Figure 1 shows the results of $LiMn_2O_4$. It is clear that the reflection is flat for the temperature region from 77 to 380 K. These results are similar to those of $LiCoO_2$ but different from $LiNiO_2$. The absolute reflection value is very close to that of $LiCoO_2$. In order to investigate the charge-discharge process in $LiMn_2O_4$, the millimeter wave reflection measurement of $Li_{1-x}Mn_2O_4$ is desired. However, as $Li_{1-x}Mn_2O_4$ is very fragile, we have not succeeded in observing $Li_{1-x}Mn_2O_4$. This remains as a future problem.

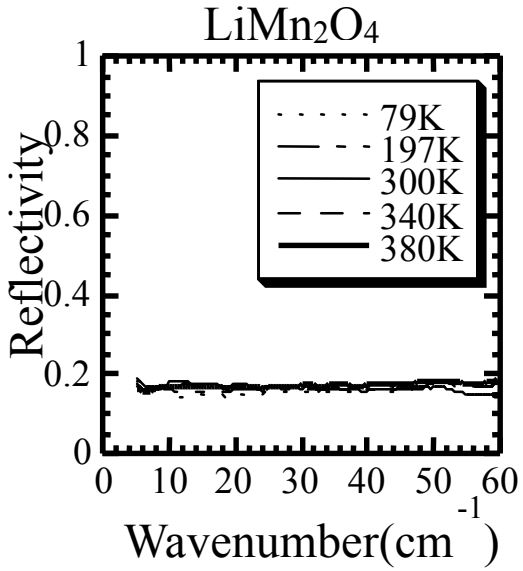

Fig. 1. Reflection spectra of $LiMn_2O_4$.

[1] H. Ohta *et al.*: UVSOR Activity Report 1996 (1997) 182.
[2] H. Ohta *et al.*: UVSOR Activity Report 1997 (1998) 128.
[3] H. Ohta *et al.*: UVSOR Activity Report 1998 (1999) 158.
[4] H. Ohta *et al.*: UVSOR Activity Report 1999 (2000) 93.
[5]H. Ohta *et al.*: UVSOR Activity Report 2000, (2001) 121.
[6] H. Ohta *et al.*: Jpn. J. Applied Phys. **39** (2000) Suppl. 39-1, 409-410.
[7] H. Ohta *et al.*: UVSOR Activity Report 2001, (2002) 138.
[8] H. Ohta *et al.*: UVSOR Activity Report 2002, (2003) 142.
[9] Y. Nagasaka *et al.*: J. Phys. Chem. Solids 64 (2003) 1949-1951.

BL-6B

Laser-induced Infrared Absorption of Carbon Nanotubes

J. Azuma, M. Itoh[A], M. Koike[A], T. Sakurai[A], M. Kamada and M. Endo[A]
Synchrotron Light Application Center, Saga University, Saga 840-8502, Japan
[A] *Faculty of Engineering, Shinshu University, Nagano 380-8553, Japan*

Since the discovery of carbon nanotube by Iijima [1], a new research field has been developed in material science. Many future applications can be expected from its interesting physical properties. For example, there are semiconducting and metallic carbon nanotubes, depending on their diameter and chirality [2,3]. The development of the sample synthesis of single-walled carbon nanotubes (SWNTs) has allowed detailed experimental studies of the electronic structure. It is important to measure the fundamental absorption of SWNTs for sample characterization. From the viewpoint of applications to electronic devices, it is also necessary to obtain the electronic properties of the metallic SWNT and of the photo-excited states in semiconducting SWNT.

In this paper, the optical absorption spectra of SWNTs prepared by two different chemical treatments are shown. The laser-induced change of the absorption spectra is also reported.

Experimentals

The absorption measurements were performed in the energy range of 400-15000 cm^{-1} with a rapid-scanning Michelson interferometer (Bruker, IFS-66V) by using a KBr or a quartz beam splitter. An HgCdTe photoconductive detector and a Si photodiode were used in the infrared and visible regions, respectively. Photo-excitation was performed by a Ti:sapphire laser (Coherent, Mira-900F) at 800 nm with 250 mW average power. The samples used in this experiment were prepared by dispersing two types of SWNT solutions onto BaF_2 substrates. One is the SWNT with iron impurity. The other is the SWNT in which iron impurity was chemically removed.

Results and Discussion

Fig. 1(a) shows absorption spectra of the two types of SWNTs at room temperature. The band-to-band transition of semiconducting SWNT is observed above 4000 cm^{-1}. On the other hand, the Drude tail of metallic SWNT appears below 3000 cm^{-1}. The absorption tail of the band-to-band transition increases slightly in the SWNT:Fe as compared with the Fe-removed SWNT. This increase is probably ascribed to the impurity state. The intensity ratio of the band-to-band transition to the Drude tail is also different between the two samples. The ratio might be changed by the difference in the chemical process of the impurity removal.

Fig. 1(b) shows the laser-induced change of the IR absorption spectra at room temperature. One can see that an additional absorption tail appears below 1000 cm^{-1}. This absorption tail is assigned to the Drude tail of the photo-excited carriers in semiconducting SWNTs. In usual, photoconductivity measurements using electrodes are required to obtain information about the photo-excited carriers. The present experiment demonstrates that it is capable to perform the photoconductivity measurement without electrodes by using tunable laser and brilliant IR light. This result is essentially important for the study on the electronic properties of SWNTs to which it is very difficult to attach the electrodes.

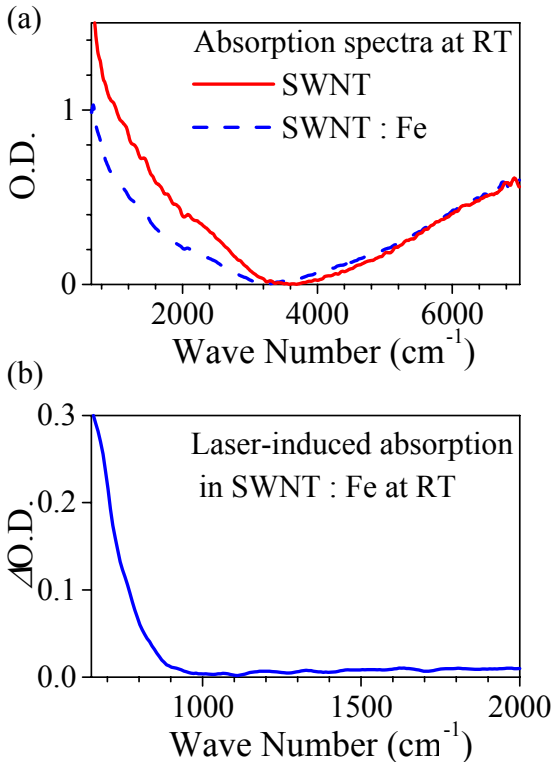

Fig.1 (a): Absorption spectra of two SWNTs. (b):Laser-induced absorption in SWNT:Fe.

The detailed analysis of the laser-induced spectral change of SWNTs is in progress. Time-resolved experiment is necessary to obtain further information about the dynamics of photo-excited carriers.

Acknowledgement

This work was supported by the CLUSTER of the Ministry of Education, Culture, Sports, Science and Technology of Japan.

[1] S. Iijima, Nature, **354** (1991) 56.
[2] X. Blasé, L.X. Benedict, E.L. Shirley, S.G. Louie, Phys. Rev. Lett., **72** (1994) 1878.
[3] J.W. Mintmire, C.T. White, Carbon **33** (1995) 893.

BL6B&7B

Optical Response of β-$Na_{0.33}V_2O_5$ and Its Electronic Structure

L. Chen, M. Matsunami, H. Okamura, T. Nanba, T. Yamauchi* and Y. Ueda*

Graduate School of Science and Technology, Kobe University, Kobe 657-8501, Japan

**Materials Design and Characterization Lab. ISSP, University of Tokyo, kasiwa 277-8581,Japan*

β-Na0.33V2O5 is one of β-vanadium bronze compounds and attractive materials because it exhibits a quasi-one-dimensional (quasi-1D) metallic behavior and a metal-insulator transition (MIT) accompanying charge ordering at around 135 K[1]. The evidence for the charge separation into V+4 and V+5 states was obtained from NMR measurements[2] Up to now, however, the electronic states due to the MIT has not been made clear. In this paper, we report the temperature dependent optical spectra around the MIT and discuss the electronic structure very close to the Ff level.

Experimental

The temperature dependence of optical reflectivity spectra $R(\omega)$ at ambient pressure was measured in the wide photon energy range from 7 meV to 30 eV in the temperature range of 8-300 K. The measurements were performed using a Fourier-transform interferometer combined with a thermal light source and synchrotron radiation source at the beam line BL6B & 7B of UVSOR, Institute for Molecular Science. The optical conductivity $\sigma_1(\omega)$and complex dielectric function $\varepsilon_1(\omega)$ were obtained from a standard Kramers-Kronig transformation of the measured reflectivity spectrum.

Results and discussions

Fig.1 shows the temperature dependence of the optical conductivity for E//b (upper) and E ⊥ b (lower). The electric resistivity data shows the conductivity in the b-axis due to the formation of a quasi-1D-chain by vanadium ions along the b-axis. Optical conductivity spectra for E//b show a clear Drude component by free carriers. The many spike structure were resolved below 0.1 eV even in the metallic phase. This means that the low density of free carriers in the conduction band which leads to the weak screening of the electric polarization for lattice vibration(phonon). On the other hand, the optical conductivity spectra for E ⊥ b shows a typical insulating profile. The onset of the interband transition locates at 0.1eV and the intense peak due to the transition from the V-3*d* initial state to the upper *p* state in the conduction band appears at 0.35 eV for E//b. On the other hand, for E ⊥ b the onset locates at 0.25 eV and the intense peak appears at 0.85 eV. This means the magnitude of the energy gap is smaller for E//b than E ⊥ b. The intense peak due to the transition from the O-2*p* state appears around 7 eV for both configuration. The same peak energy suggests the O-2*p* state has no anisotropy in band scheme.

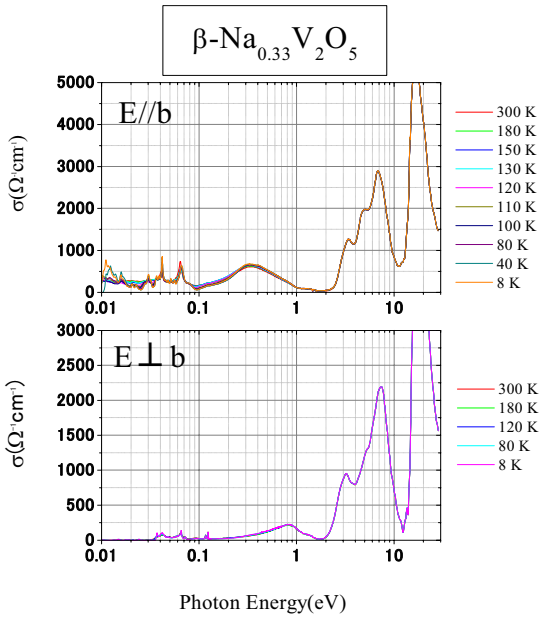

Fig. 1. The optical conductivity $\sigma_1(\omega)$ for E//b (upper) and E ⊥ b(lower).

[1] T,Yamauchi *et al*., Phys.Rev.Lett. 89(5) 057002-1 (2002).
[2] M.Itoh, *et al*. J.Phys.Soc.Jpn. 69 155(2000).

BL6B

Infrared spectroscopy on CeSb at high pressure

T. Nishi[1], Y. Mori[2], Y. Sumida[2], Y.S. Kwon[3,4], H. Kitazawa[5], S. Kimura[1,3]

[1]*Department of Structural Molecular Science, Graduate University of Advanced Studies, Okazaki 444-8585, Japan*

[2]*Department of Physics, Okayama University of Science, Okayama 700-0005, Japan*

[3]*UVSOR Facility, Institute for Molecular Science, Okazaki 444-8585 Japan*

[4]*Department of Physics, SungKyunKwan University, Suwon 440-746, South Korea*

[5]*Nanomaterials Laboratory, National Institute for Materials Science, Tsukuba 305-0047, Japan*

CeSb has a complex magnetic phase diagram not only under magnetic fields [1] but also at high pressure. [2] The fundamental magnetic structure is double ferromagnetic layer along magnetic fields, for instance the magnetic structure at the antiferromagnetic state below 9 K at B = 0 T, P = 0 GPa is ++--, where +(-) is the ferromagnetic layer along the magnetic field. At P = several GPa, single-layer antiferromagnetic phase (+-) appears. In the phase, the electric resistivity enhances one order higher than that at ambient pressure and it is strongly reduced by magnetic fields. [3] To investigate the electronic structure from which such anomalous physical property originates, the infrared reflection spectroscopy at high pressure was performed.

The experiment was done using an IR microscope and a diamond anvil cell (DAC) mounted on a liquid-helium-flow-type cryostat. The sample size was about 0.2 × 0.2 × 0.05 mm^3. Because of the high brilliance of IR synchrotron radiation, The IR reflection from a sample in the DAC can be detected clearly.

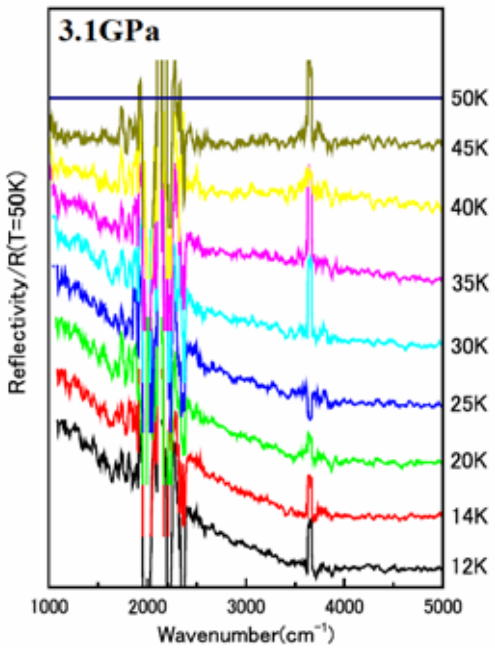

Fig. 1. Temperature dependence of relative reflectivity spectrum of CeSb at P = 3.1 GPa.

The obtained temperature dependence of the relative reflectivity spectrum of CeSb at P = 3.1 GPa are shown in Figure 1. The spectra are the reflectivity at each temperature divided by that at 50 K. Below 25 K, since all spectra are similar to one another, the electronic structure in the energy region as well as the magnetic phase does not change. Above 25 K, the spectrum gradually changes and then above 40 K the spectrum becomes flat. The temperature dependence is clearly indicated in the reflectivity at ω = 3000cm^{-1} as shown in Figure 2. The slope changes at $T1$ = 25 and $T2$ = 40 K. This means that the electronic structure changes at these temperatures. This result originates from the magnetic phase diagram. According to the neutron scattering data [2], two phase boundaries appear at this pressure. The $T1$ and $T2$ are same as those detected by the neutron scattering.

The reflectivity spectra at the temperatures between $T1$ and $T2$ are gradually changes. This indicates that the magnetic interaction, in this case the *pf* mixing effect, gradually changes with temperature. The origin seems to the second order transition observed in CeBi at ambient pressure. [4]

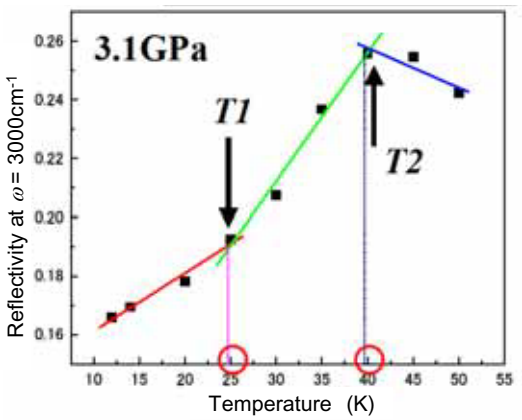

Fig. 2. Temperature dependence of the reflectivity intensity at ω = 3000cm^{-1} of CeSb at P = 3.1 GPa.

[1] S. Kimura *et al.*, J. Phys. Soc. Jpn. **71** (2002) 2200.
[2] Osakabe *et al.*, Acta Phys. Pol. B **34** (2003) 1469.
[3] N. Môri *et al.*, JJAP Series 8 (1993) *p.* 182.
[4] S. Kimura *et al.*, submitted.

BL6B

Far-infrared Reflectivity Measurement of $SrTiO_3$

H. Okamura, M. Matsubara, T. Nanba, K. Tanaka*
Graduate School of Science and Technology, Kobe University, Kobe 657-8501, Japan.
**Graduate School of Science, Kyoto Univeristy, Kyoto 606-8502, Japan*

$SrTiO_3$ (STO) has many interesting properties, and has been studied by condensed matter physicists for nearly half a century. STO is an insulator with an energy gap of about 3.4 eV and a static dielectric constant ε_0 of about 200 at room temperature. With decreasing temperature, ε_0 increases, and reaches ~ 20000 at liquid helium temperature. A Curie-Weiss plot suggests a Curie temperature of ~ 30 K, but it does not undergo a phase transition to a ferroelectric state. This absence of a ferroelectric transition in STO has been attributed to large quantum fluctuations of electric dipole moment, or equivalently strong zero-point oscillations of the ions. However, a clear softening of an optical phonon has been observed with infrared spectroscopy, which demonstrates a tendency toward ferroelectric ordering. Recently, it has been reported that a photoexcitation of STO across the band gap using UV light further increases ε_0 by a factor of 2 to 100 depending on the conditions of the photoexcitation [1,2]. This photo-induced enhancement of the dielectric properties has attracted a lot of interest, and several models have been proposed.

Besides the enhancement of dielectric properties at low temperatures, STO has other unique features. First, it gives a strong, white luminescence over a wide visible range by UV photo-excitation [4]. Since the band gap of STO is 3.4 eV, this means that the photo-generated carriers in STO experience large energy relaxation processes before recombination. Possibilities of polarons and self-trapped excitons have been discussed. Second, STO exhibits a very strong photoconductivity below the structural phase transition at 105 K [5]. At low temperatures, photo-excitations increase the conductivity of STO by several orders of magnitude. It has been suggested that the photoconductivity and the photo-enhancement of the dielectric properties are closely related to each other.

In order to probe the lattice dynamics of STO, we have carried out far-infrared reflectivity measurement of STO down to 10 cm^{-1} at BL6B of UVSOR. The STO sample used had a (110) surface. Figure 1 shows the results. The spectra below ~45 cm^{-1} were measured at BL6B using the synchrotron radiation source and a Martin-Puplett type interferometer, while those above 45 cm^{-1} were measured at Kobe University using a conventional source and a Michelson type interferometer. At 295 K, there is a broad "dip" in the reflectivity below ~100 cm^{-1}. This corresponds to an optical phonon, which is very broad due to strong damping. The point where the reflectivity begins to decrease, ~100 cm^{-1} for 295 K, approximately corresponds to the frequency of the optical phonon. As the temperature is lowered, the dip becomes narrower and shallower. This result clearly demonstrates softening of the optical phonon. Although there is a previous report on the temperature-dependent soft phonon of STO [6], our present result covers much wider temperature and photon energy range. To make more detailed analyses on the data, we plan to perform the Kramers-Kronig analysis on the reflectivity data.

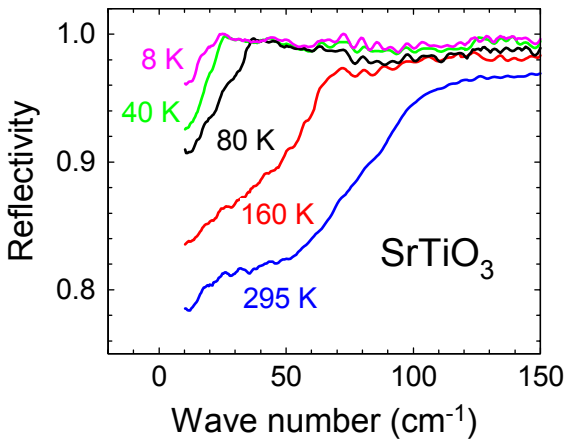

Fig. 1. The reflectivity spectra of $SrTiO_3$ at several temperatures. The spectra below 45 cm^{-1} were measured at BL6B, and those above were measured at Kobe University.

[1] K. A. Muller and H. Burkard, Phys. Rev. **B** 19, 3593 (1979).
[2] M. Takesada, T. Yagi, M. Itoh, S. Koshihara, J. Phys. Soc. Jpn. **72**, 37 (2003).
[3] T. Hasegawa, S. Mouri, Y. Yamada, K. Tanaka, J. Phys. Soc. Jpn. **72**, 41 (2003).
[4] L. Grabner, Phys. Rev. **177**, 1315 (1969).
[5] H. Katsu, H. Tanaka, T. Kawai, Jpn. J. Appl. Phys. **39**, 2657 (2000).
[6] A.S. Barker and M. Tinkham, Phys. Rev. **125**, 1527 (1962).

BL7B

Reflectivity Spectra and Electronic Structure of α-$LiIO_3$ Crystals

M. Kitaura, S. Kawabata[A], M. Kato[A], S. Matsumoto[A], H. Nakagawa[A], and M. Itoh[B]

Fukui National College of Technology, Sabae 916-8507

[A]*Department of Electrical and Electronics Engineering, Fukui University, Fukui 910-8507*

[B]*Department of Electrical and Electronic Engineering, Shinshu University, Nagano 380-8553*

Lithium iodate ($LiIO_3$) has two crystal structures, hexagonal (α-type) and tetragonal (β-type) ones, under normal conditions. From the viewpoint of technological application, the α-$LiIO_3$ crystal receives intense attention as a promising candidate for photorefractive (PR) substance. It has been generally accepted that the PR effect arises from trapping of photo-induced electrons and/or holes at some deep levels. The origin of the trap states is of great interest, but it has not yet been clarified in α-$LiIO_3$. This material is also known to be a quasi one-dimensional ionic conductor. The mobile ionic species are mainly lithium ions, the thermal migration of which is greatly enhanced by the super ionic phase transition at the temperature T= 243 K. As pointed out in Ref. [1], this phenomenon has a close relationship with the weakening of PR properties. It is thus supposed that interstitial Li^+ ions or Li^+ vacancies are linked to formation of the trap states responsible for the PR effect.

The optical spectra of pure crystals are necessarily required to study the effect of imperfections on the electronic structures. In pure α-$LiIO_3$, optical spectra have been investigated in the energy region lower than the fundamental absorption edge at around 4 eV. In order to understand the electronic structure, it is important to clarify the optical spectra in the energy region above 4 eV.

In the present study, polarized reflectivity spectra of α-$LiIO_3$ were measured in the energy range of 3-30 eV at room temperature. They were obtained for the polarization parallel ($E\|c$) and perpendicular ($E\perp c$) to the c-axis. The origin of the structures in the spectra is explained on the basis of the results of the DV-$X\alpha$ calculation.

Experiment

The crystals of α-$LiIO_3$ were grown by dissolving stoichiometric quantities of reagent grade iodic acid and lithium carbonate in distilled water. The obtained crystal was transparent, with a size of 6 mm in length and 2 mm in diameter.

The measurements of reflectivity spectra were carried out at BL7B using a 3-m normal incidence monochromator. The band-pass was set to be less than 0.3 nm. The incident angle of SR light for the sample surface was held at 15 degrees. The incident and reflected light were detected using a calibrated silicon diode sensor (IRD AXUV−100). The absolute values of reflectivity were determined by reference to the refractive indices at 3.5 eV in Ref. [2].

Results and Discussion

Figure 1 shows reflectivity spectra of α-$LiIO_3$ for $E\|c$ and $E\perp c$ configurations, which are indicated by solid and broken lines, respectively. The spectra exhibit remarkable difference in reflectivity. The spectral shape is also different especially in the energy region below 10 eV. In both configurations, there exist broad structures above 10 eV.

Our cluster calculation revealed that the valence band (VB) of α-$LiIO_3$ is built of the O 2p states with small admixture of I 5s and 5p characters. The base width of the VB is about 5 eV. The outermost core levels, composed of I 5s, O 2s and 2p orbitals, appear around −10 eV. On the other hand, the bottom of the conduction band (CB) is composed of Li 2s and I 5p orbitals. The higher-lying states are formed by Li 2p orbitals. The band gap is calculated to be 6.15 eV.

The reflectivity spectra are composed of two parts: I (5-10 eV) and II (10-20 eV). According to results of the present calculation, the structures in part I are ascribed to the electronic transitions from the VB of O 2p to the lower CB of Li 2s. The transitions of O 2p → I 5p are expected to be weak in the part I, because this type of transitions are electric-dipole forbidden. The structures in part II originate from the transitions from the top of the VB to the Li 2p conduction states and those from the outermost core levels to the lower CB.

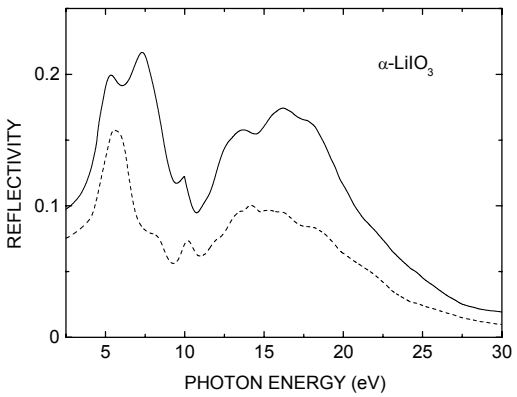

Fig. 1. Reflectivity spectra of α-$LiIO_3$ at room temperature for $E\|c$ (solid line) and $E\perp c$ (broken line) .

[1] J. Xu, X. Yue, and R. A. Rupp, Phys. Rev. B, **54** (1996) 16618.

[2] K. Takizawa, M. Okada, and S. Ieiri, Opt. Commun., **23** (1977) 279.

BL7B

Reflectivity Spectra of Second-Group Metal Tungstate Crystals

M. Fujita
T. Maruyama*, S. Takagi*, N. Fujita*, M. Itoh*
Japan Coast Guard Academy, Wakaba, Kure 737-8512
** Department of Electrical and Electronic Engineering, Shinshu University, Nagano 380-8553*

The second-group metal tungstate crystals are important materials because of their uses as a scintillation detector in medical applications, solid laser hosts and optical fibers. They crystallize into scheelite or wolframite structures. In the present study, reflectivity spectra of $CaWO_4$ and $BaWO_4$ crystals with scheelite structure and $CdWO_4$ with wolframite structure were measured in order to investigate the electronic structures of these tungstate compounds.

Experiment

Reflection measurements were carried out for oriented crystals of $CaWO_4$ and $CdWO_4$, and for unoriented crystal of $BaWO_4$ using a 3-m normal incidence monochromator at BL7B.

Results and Discussion

Figure 1(a) shows reflectivity spectra of $CaWO_4$ and $BaWO_4$ at 10 K. For each crystal, the lowest absorption band is observed at 6.0 eV. The band is rather broad compared with the exciton peak of $PbWO_4$ [1]. Several broad structures are seen in the region of 7–15 eV. In $CaWO_4$, the polarization dependence of the lowest peak is weak, while the structures in the 7–15 eV region show distinct dichroism. In $BaWO_4$, spectral features above 15 eV resemble those of BaF_2, indicating that the optical transitions from the Ba 5*p* core levels are involved in this high-energy region.

Reflectivity spectra of $CdWO_4$ crystal are shown in Fig. 1(b). In the 4–7 eV region is observed a broad band with weak fine structures. The small peak at 4.3 eV is probably assigned to the lowest exciton transition. Several sharp peaks are observed in the 7–11 eV region. In contrast to the case of $CaWO_4$, the spectral features below 7 eV depend strongly on the polarization. The difference in optical spectra is clearly seen between the scheelite and wolframite crystals.

The electronic structures of $CaWO_4$ and $CdWO_4$ were calculated by the DV-$X\alpha$ method. In Fig. 2 are shown the results for $[Ca_4WO_4]^{6+}$ and $[CdW_4O_{16}]^{6-}$ clusters. The valence band is mainly built of the O 2*p* state and the conduction band is composed of the W 5*d* state for both structures. In scheelite crystals, W ions are in almost tetrahedral O-ion cages to form WO_4 complex, which are isolated from each other. In wolframite crystals, W ions are in distorted WO_6 octahedra, which form chains by edge sharing. The difference of the spectral features between scheelite and wolframite might be attributed to the different coordination of O ions around W ions.

[1] M. Fujita, M. Itoh, M. Horimoto and H. Yokota, Phys. Rev. **B** 65 (2002) 195105.

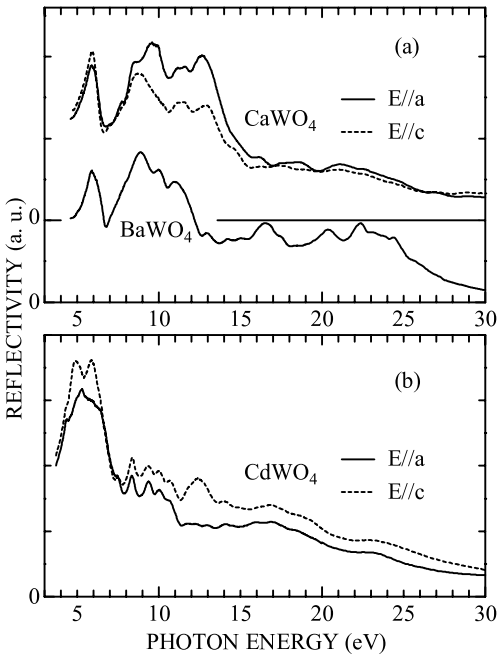

Fig. 1. Reflectivity spectra of (a) $CaWO_4$ and $BaWO_4$, and (b) $CdWO_4$ at 10 K.

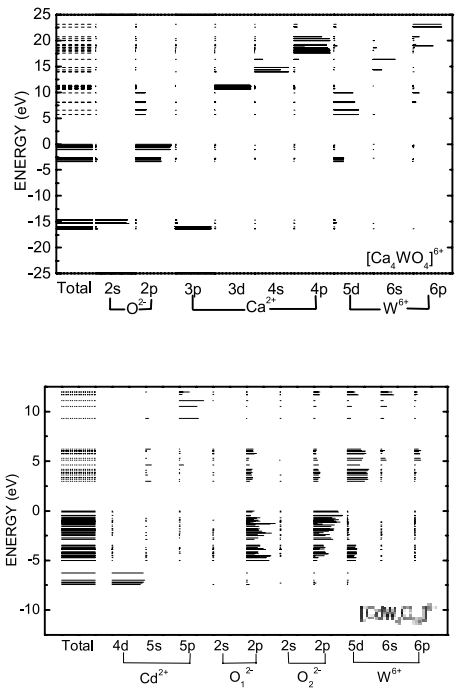

Fig. 2. Energy diagrams of $[Ca_4WO_4]^{6+}$ (upper) and $[CdW_4O_{16}]^{6-}$ (lower) clusters calculated by the DV-$X\alpha$ method.

BL7B

Characterization of UV Detectors with n-AlGaN on AlN Epitaxial Films

K. Hiramatsu[1], Y. Shibata[1], H. Yasukawa[1], A. Motogaito[1], H. Miyake[1], Y. Ohuchi[2], K. Tadatomo[2], T. Nomura[3], Y. Hamamura[3] and K. Fukui[4]

[1]*Dept. of Electrical and Electronic Engineering, Mie University, Tsu 514-8507 Japan*

[2]*LED Business Development Dept., Mitsubishi Cable Co. Ltd., Itami 664-0027 Japan*

[3]*Core Technology Center, Nikon Corporation, Sagamihara 228-0828 Japan*

[4]*Research Center for Development for Far-Infrared region, Fukui University, Fukui 910-8507 Japan*

Characterizations of transparent Schottky barrier n-$Al_{0.5}Ga_{0.5}N$ UV detectors on AlN epitaxial layer in the vacuum UV (VUV) region using synchrotron radiation are described. The high responsivity spectra were realized by using n-AlGaN Schottky UV detectors compared to GaN UV detectors.

Our group has reported on the responsivity spectra of GaN UV detectors in VUV region [1, 2] but they are lower than that in near UV region. To improve it, AlGaN UV detectors are attractive devices because of larger band gap compared with GaN. Furthermore, the advantages of III-nitride materials that are wide band gap and radiation proof will bring out the possibilities of better performance for detection of SX light instead of Si photodiode. If UV detectors can detect VUV and SX light, they will be used in the steppers for future photolithography systems.

In this report, characterization of GaN and AlGaN UV detectors with a transparent electrode in the VUV and SX region using synchrotron radiation are carried out and the comparison of device performance for these devices are described. These AlGaN UV detectors were fabricated on AlN epitaxial layer on (0001) sapphire substrate as shown in Figure 1. The latter structures consists of a 1-μm-thick n-$Al_{0.5}Ga_{0.5}N$ layer (n=2.0×10^{18} cm^{-3}) on (0001) AlN on sapphire substrate. These layers are grown by metalorganic vapor phase epitaxy (MOVPE). The details of growth of AlGaN on AlN are described in ref. [3-5]. The transparent Ni/Au Schottky electrode is formed on n-AlGaN layer. Its diameter is 0.8 mm. The transmittance of Ni/Au electrode is about 0.4-0.5 in the VUV region. The responsivity of UV detectors is estimated by measuring the photocurrent illuminating SR at the beam line 7B (BL7B). UV detectors are illuminated with the monochromatic light, which is between $h\nu$=2.2 eV (λ=564 nm) and $h\nu$=25 eV (λ=50 nm).

The responsivity spectra of $Al_{0.5}Ga_{0.5}N$ UV detectors in near UV and VUV (2-25 eV) are also characterized. Figure 5 shows the responsivity spectra of AlGaN UV detectors. In this figure, to compare the responsivity between GaN and AlGaN UV detectors, the responsivity spectra of unit illuminating area are shown. The band gap energy of $Al_{0.5}Ga_{0.5}N$ is 4.7 eV. Thus, the photon which energy is less than 4.7 eV is not absorbed. At 4.7 eV, the sharp cut-off characteristic is observed. The ratio of responsivity between UV and VIS regions is about 5,000 – 10,000 like GaN UV detectors. The absolute responsivity at 5.0 eV and VUV region is 0.035 A/W and 0.015 A/W, respectively. Compared with responsivity spectra of GaN UV detectors, the high responsivity in VUV region is realized using AlGaN UV detectors. For example, at 6.5 eV (193 nm, corresponding to light emitting wavelength of ArF lasers), the responsivity of AlGaN (60 mW/A/mm^2) is 16 times as high as that of GaN (3.7 mW/A/mm^2). Therefore, $Al_{0.5}Ga_{0.5}N$ UV detectors have possibilities to detect VUV light with higher responsivity by improving crystal quality of AlGaN layer and device structures in the future.

[1] A. Motogaito et al., Jpn. J. Appl. Phys. 40 (2001) 368.

[2] A. Motogaito et al., Phys. Stat. Sol. (a) 188 (2001) 337.

[3] Y. Kida et al., Phys. Stat. Sol. (a) 194 (2002) 498.

[4] Y. Kida et al., Phys. Stat. Sol. (c) 0 (2003) 2128.

[5] H. Miyake et al., Phys. Stat Sol. 200 (2003) 151.

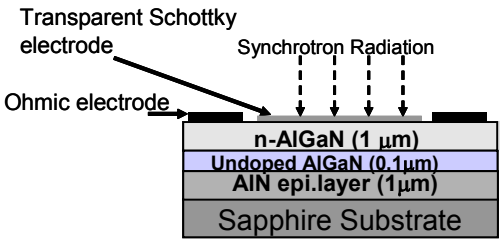

Fig. 1 The Schematic drawing of AlGaN UV detectors.

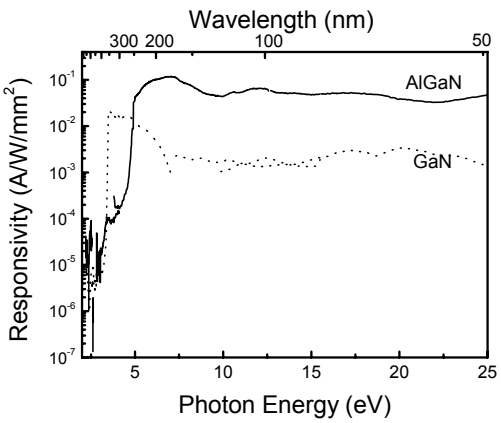

Fig. 2 Responsivity spectra of AlGaN UV detectors compared with GaN UV detectors [2].

BL7B

The 4*f*-5*d* Electronic Excitations in Reflectivity Spectra of *Ln*MnO_3

H. Kuroe, Y. Yagi, Y. Hirobe, H. Kuwahara and T. Sekine
Department of Physics, Sophia University, Tokyo 102-8554 Japan.

The orthorhombic $LaMnO_3$ has been extensively studied because this system has many kinds of interesting phenomena such as the orbital and antiferromagnetic orders. Recently, Ravindran *et al.* calculated the reflectivity spectra of $LaMnO_3$ with a generalized-gradient-corrected relativistic full-potential method [1]. They reproduced the reflectivity spectra observed by Jung *et al.* [2], Arima *et al.* [3] and Takenaka *et al.* [4]. Recently, the trivalent lanthanide ion (Ln^{3+} ion) dependence of the magnetic property also attracts much attention. [5,6]. When the ionic radius of Ln^{3+} ion is small enough, the crystal structure becomes hexagonal $YMnO_3$-type. In this work, we measured the reflectivity spectra in *Ln*MnO_3 from visible to vacuum ultraviolet light.

Experiments

The single crystals of *Ln*MnO_3 (*Ln* = Pr, Sm, Eu, Tb, Dy, Ho, Er and Yb) were prepared by floating-zone method. According to RIETAN2000 analysis of x-ray powder diffraction, the crystals of *Ln* = Yb, Er and Ho have a hexagonal $YMnO_3$-type structure and those of *Ln* = Tb, Eu, Sm and Pr have a orthorhombic $GdMnO_3$-type one. The single crystal of *Ln* = Dy contains the 24% $YMnO_3$-type and 76% $GdMnO_3$-type phases. The crystal axes were checked by Laue pattern. The samples were cut and polished with 0.05-μm Al_2O_3 powder carefully. The post annealing from 1000 ˚C with a cooling rate of 10 ˚C/hour was performed in O_2. The reflectivity spectra in the paramagnetic phase were measured with the 3-m normal incident monochromator in BL7B of UVSOR. We set the polarization of the light along to the pseudo-cubic lattice vector.

Results and Discussion

Figure 1 shows the observed spectra between 1.2 and 15 eV in *Ln*MnO_3 (*Ln* = Pr, Sm, Eu, Tb, Dy, Ho, Er and Yb) in addition to those reported in Refs. [1-4]. The electronic configurations of the trivalent ions are $4f^0$ in La^{3+}, $4f^2$ in Pr^{3+}, $4f^5$ in Sm^{3+}, $4f^6$ in Eu^{3+}, $4f^8$ in Tb^{3+}, $4f^9$ in Dy^{3+}, $4f^{10}$ in Ho^{3+}, $4f^{11}$ in Er^{3+} and $4f^{13}$ in Yb^{3+}. The bold lines indicate the experimental conditions (grating: G1, G2 and G3), filters: O53, Pyrex(P), Quartz(Q) and LiF). The reflectivity peaks indicated by arrows around 1.2 and 3.5 eV in Fig. 1 are due to Mn–O charge-transfer process [3,4]. The line shapes of these peaks in the hexagonal crystals are similar to those in the orthorhombic ones. In our measurements, the peak structure from the intraionic 4*f* – 4*f* excitation, for example the structure between 4 and 5 eV when *Ln* = Pr, was superimposed on the peaks due to the Mn-O charge-transfer process.

We observed the large peaks between 3 and 10 eV when *Ln* = Yb, Er, Ho, Dy and Tb. We assigned them to the reflectivity peaks due to the electronic excitation between $4f^n$ and $4f^{n-1}5d$. This process is electric-dipole allowed [7]. This 4*f* – 5*d* electronic excitation process was also observed in emission spectra in lanthanide-doped materials [8]. These peaks do not come from the breakdown of the selection rule, because the reflectivity peaks were clearly observed even when *Ln* = Tb, which has the $GdMnO_3$-type crystal structure. In the cases of *Ln* = Pr, Sm and Eu, we did not observe the peaks due to the 4*f* – 5*d* excitation process.

We also observed the reflectivity peaks due to electronic excitation between O2*p* and *Ln*5*d* orbitals which was reported in Ref. [3].

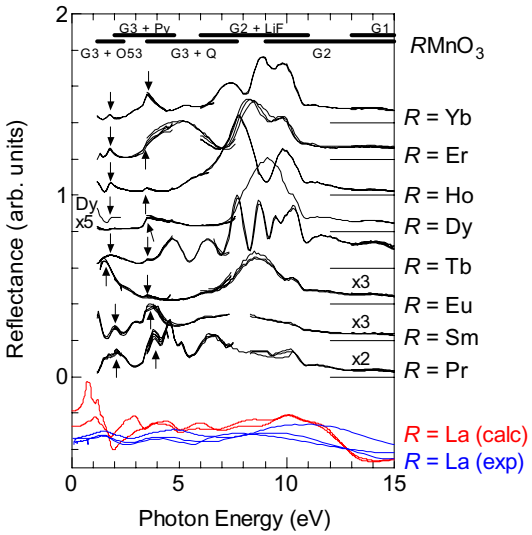

Fig. 1. Observed and calculated reflectivity spectra. The bold lines indicate the experimental conditions. The red and blue curves are the reflectivity spectra reported in Refs. [1-4]. The peaks indicated by arrows are due to the Mn-O charge-transfer exictation.

[1] Ravindran *et al.*, PRB **65**, 064445 (2002).
[2] J. H. Jung *et al.*, PRB **55**, 15489 (1997).
[3] Arima *et al.*, PRB **48**, 17006 (1993).
[4] K. Takenaka *et al.*, JPSJ. **68**, 1828 (1999).
[5] T. Kimura *et al.*, PRB **68**, 060403 (2003).
[6] T. Kimura *et al.*, Nature **426**, 55 (2003).
[7] M. F. Reid *et al.*, J. Alloys. Comp. **344**, 240 (2002).
[8] R. T. Weigh *et al.*, thesis (1999) and their references; R. T. Wegh *et al.* PRB **60**, (1999) 10822.

BL7B

UV Reflection Spectra of Nanocrystalline β-$FeSi_2$

K.Takarabe, Y. Mori
K.Fukui*
T.Yoshitake**
Okayama University of Science, Okayama 700-0005 Japan
**Fukui University, Bunkyo 3-9-1, Fukui 910-8507 Japan*
***Department of Applied Science for Electronics and Materials, Kyushu University, 6-1 Kusaga, Fukuoka 816-8580 Japan*

Iron disilicide, β-$FeSi_2$, has attracted much attention as promising material for optoelctronic applications. β-$FeSi_2$ emits light of 1.55 μm(0.8 eV) suitable for SiO_2 optical fiber communicatios and can be grown epitaxially on Si. β-$FeSi_2$ is also known to be a Kankyo semiconductor(ecologically friendly semiconductor). A well annealed thin-film sample shows a highest hole mobility of 13000cm^2/Vs at 50 K, which exceeds the electron mobility. Room -temperature electroluminescence action has been already reported.

There are a growing number of studies of basic properties of β-$FeSi_2$. For example, Filonov et al. calculated the dielectric functions in a wide range of photon energies up to 5 eV, and compared these with the ellipsometric experiments. Takarabe et al. performed a first-principles calculation of the optical properties of β-$FeSi_2$ focusing on the near-edge absorption coefficient and reported on the high-pressure measurement of its absorption up to 5 GPa, and discussed the low pressure coefficient of the direct absorption edge of 15.9 meV/GPa, one seventh of that of GaAs, is the negative deformation potential of the valence-band maximum and due to the second largest bulk modulus of 243.5 GPa among common semiconductors. [1]

Exploration of advanced properties extends from the single crystal to nanocrystalline β-$FeSi_2$ in which we expect a quantum confinement effect and an increase of absorption coefficient near and below the band gap.

Sample

Pulsed-laser deposition(PLD) was applied to prepare nanocrystalline β-$FeSi_2$. This method produces a high-energitic particles and a quench of these particles on a low temperature substrate results in the amorphous and nanocrystalline β-$FeSi_2$[2].

Reflection spectra of nano β-$FeSi_2$

Reflection spectrum of the nano β-$FeSi_2$ shows some slightly broad but still developed reflection bands as shown in Fig. 1, it is understood as a finger print of a crystalline state with some degree of amorphous state. The structures are denoted from S0 to S4. In the reflection spectrum of the crystalline β-$FeSi_2$ measured in the energy of visible region, the well structured reflection band appears below 2.5 eV and also in the calculated reflectivity with a first-principles calculation. However, this structure is completely smeared out in the nano β-$FeSi_2$. This indicates that the amorphous state affects strongly on the lower energy dielectric function than the higher-energy region. The structure at about 5 eV in the calculated reflectivity corresponds to the observed rise of reflectivity at the reflection band S0. One of the possibilities to interpret the S0 structure is the broadening of the calculated reflection band at 5 eV. The sharp reflection band at 20 eV in the calculated spectra is the plasma oscillation of the valence band of the crystalline β-$FeSi_2$. This is strongly damped in the measured reflectivity, although the S4 structure is close in energy. The structures S1 to S3 in the measured reflectivity have no counter part in the calculated reflectivity. In this sense this fact is inherent to the nanocrystalline β-$FeSi_2$.

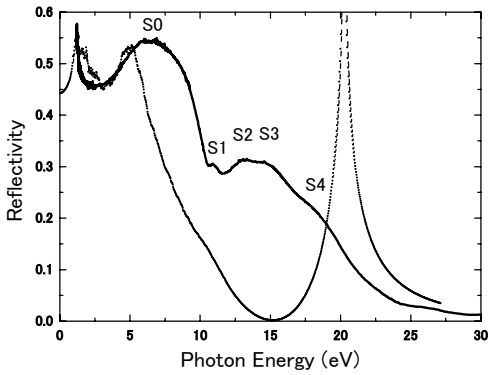

Fig. 1. Measured and calculated reflection spectra of nanocrystalline and crystalline β-$FeSi_2$, respectively.

The measured reflection spectrum of the nanocrystalline β-$FeSi_2$ shows a prominent difference from that of the crystalline state, at least the calculated spectra. The study to characterize the nanocrystalline state is at very early stage but this report shows the UV reflectivity is useful for this study.

[1] K.Takarabe et al., Phys. Rev.B, 65, 16215(2002); Y.Mori et al., phys. stat. sol(b) 235, 302(2003), and references therein.
[2]T.Yoshitake et al., Appl. Phys. Lett., 83, 3057(2003).